THE UNIVERSITY OF SOUTHAMPTON

THE RHEOLOGY OF HIGH GAS VOLUME FRACTION AQUEOUS FOAMS

A Thesis submitted for the Degree of

Master of Philosophy

by Mark Andrew Camp

May 1988

UNIVERSITY OF SOUTHAMPTON

ABSTRACT

FACULTY OF ENGINEERING AND APPLIED SCIENCE

MECHANICAL ENGINEERING

Master of Philosophy

THE RHEOLOGY OF HIGH GAS VOLUME FRACTION AQUEOUS FOAM

by Mark Andrew Camp

There is much interest within the oil industry in the use of foams in oil recovery processes. This is principally because of the unusual properties which foams possess, particularly their rheology. The main aim of this study has been to investigate wall slip and its effects in the measurement of foam flow properties. The experiments have been performed in a specially adapted concentric cylinder rheometer. The rheometer allows a constant flow of foam through the measuring system, so as to minimise ageing effects due to decay of the foam structure.

Slippage at the walls of the rheometer has been shown to make a significant contribution to the measured rheological properties of foams. Neglecting this phenomenon leads to serious errors in the deduced flow properties. The viscosity of bulk foam may be seriously underestimated if wall slip effects are not taken into account. Once the flow data are corrected for the effect of wall slip the existence of a yield stress for foam is apparent. Wall slip layer thicknesses have been calculated and found to be of the order of 1 to 3μm, they appear to be influenced by the foam quality, bubble size and applied shear field acting on the foam.

The overall rheology of foam results from a complex interplay of flow both in the bulk foam and in the slip layers at the rheometer walls. This would seem to go a long way to explaining the dependence of observed foam rheology on the geometry of the measuring system reported in the literature. In calculations of foam flow properties, particularly in scaling-up laboratory measurements, it will be important to allow for the wall slip effect, specifically considering variations in surface area to volume ratios between the differing flow enviroments.

ACKNOWLEDGEMENTS

I would like to express my gratitude to the British Petroleum Company for permission to publish the work contained in this dissertation. I would also like to thank the following for their guidance and support during the course of the study, Dr's Ian Callaghan, Ian Livsey and Ernst Neustadter of the British Petroleum Co. and Dr J.R.Calvert my supervisor from Southampton University.

Thanks also go to Mr. Neil Martin for all his help in the preparation of this document.

M.A.Camp

CONTENTS.

Figures and Tables

GLOSSARY OF TERMS

d = Average cell diameter, m

r = Distance from the common axis of the cylinders, m

Δr = Bubble wall thickness, m

r_b = Average bubble radius, m

R_1, R_2 = Radius of the inner, outer cylinders, m

s_1, s_2 = Shearing stress at the surface of the inner, outer cylinders, N/m^2

ω = Angular velocity of the fluid, rad/s

T = Torque per unit length of the cylinders N

V_g = Volumetric flowrate of gas, m^3/s

V_l = Volumetric flowrate of liquid, m^3/s

β = Coefficient of slip, defined;

angular slip velocity = β x shearing stress, $rad.m^2/N.s$

γ = Shear rate within the fluid

δ_w = Slip layer thickness, m

η = Fluid viscosity, $N.s/m^2$

ξ = Bingham plastic index

τ = Shearing stress within the fluid, N/m^2

τ_b = Bingham yield value, N/m^2

τ_y = Yield stress, N/m^2

ϕ = Foam quality

ψ = Fluidity function, defined;

rate of shear = ψ x shearing stress, $m^2/N.s$

Ω = Angular velocity of the rotating cylinder, rad/s

Ω_ψ = Angular velocity of the rotating cylinder due to fluidity, rad/s

Ω_s = Angular velocity due to slip, rad/s

$s = \frac{s_1+s_2}{2}$, Mean shearing stress, N/m^2

$$\varepsilon = \frac{s_1 - s_2}{2s} = \frac{(R_2^2 - R_1^2)}{(R_2^2 + R_1^2)}$$

$$u = \frac{\Omega_\psi}{s} \text{ , rad.m}^2\text{/N.s}$$

1.INTRODUCTION.

Within the oil industry there is much interest in the use of foams for processes related to oil recovery. This interest has arisen because of the unusual properties which foams exhibit. They are very much more viscous than either of their constituent parts and transport suspended particulate matter very well. These properties have been exploited in the areas of enhanced oil recovery, reservoir fracturing, gas storage, well workover and drilling. In these applications the rheological properties of foams are of great importance. This has resulted in a good deal of research work as evidenced by a recent review by Heller and Kuntamukkula (1).

In this excellent review the authors have highlighted the apparent dependence of foam viscosity on the geometry of the experimental apparatus, which has been observed by many authors (1,2,3,4). They suggest that slip at the rheometer walls is a major contributory factor to this anomaly. Although the existence of wall slip in foam flow is widely recognised, it is seldom given serious consideration or experimentally investigated, despite the available methods (5,6). However, these methods require non-standard equipment and involve a considerable amount of practical effort and calculation. This may be a reason why many workers are unwilling to embark on such a study.

The principal aim of this work has been to address the question of wall slip in the measurement of foam rheology, using the method proposed originally by Mooney (5,6). Mooney has described methods for explicitly determining slip contributions in both concentric cylinder and capillary types of rheometers, it is the method for concentric cylinders used herein.

This study of foam rheology has been carried out in a specially adapted concentric cylinder rheometer. The adaptions, made to the rheometer, have enabled the individual contributions of wall slip and bulk flow to be evaluated in accordance with Mooney's theory.

Another major problem perceived by some observers in the use of rotational viscometers is that a fixed amount of foam sample is contained in the instrument (1). Due to effects such as foam collapse and drainage the time of shearing will have a pronounced effect on the torque readings obtained with these instruments. In this study the problem has been addressed by the development of a flow through measuring system, which means the foam undergoing shear may be considered as a 'steady state' material, thus minimizing ageing effects due to time.

The results cover a range of foam qualities (% gas volume fraction) from 70-98%. They show that the contribution of wall slip to the overall measurements is considerable, and increases in importance with the gas volume fraction. If it is ignored this phenomenon will lead to an underestimation of the resistance of foam to flow deformation (viscosity). The foams also possess a measurable yield stress which is masked by the existence of the slip at the walls. The uncorrected data show foam to behave as a pseudoplastic fluid, whereas the data corrected for slip contributions show the foam to be plastic in nature. At foam qualities greater than 80% the rheological behaviour becomes a complex phenomenon resulting from a redistribution of continuous phase (water) in the foam. The net result of this is a shear induced thickening of the wall slip layers. The slip layer thicknesses were found to be in agreement with other experimental values reported (7,8), and are of the order of a few micrometres.

The work contained within this dissertation is solely that of the author, except where acknowledgement is given to others, and has not been submitted for consideration in respect of any other degrees.

2.THEORY

2.1 Mooney's method and its application to actual measurements

This section details the theory behind Mooney's method (5) for determining slip effects in concentric cylinder rheometry, and shows how this method may be used to obtain the true rheological characteristics of the material under investigation.

The rate of shear in a concentric cylinder rheometer is given by;

$$r\frac{d\omega}{dr} \tag{2.1}$$

The differential equation for the angular velocity of the fluid is;

$$r\frac{d\omega}{dr} = \tau\psi \tag{2.2}$$

Since

$$\tau = \frac{T}{2\pi r^2} \tag{2.3}$$

then

$$\frac{d\omega}{dr} = \frac{T\psi}{2\pi r^3} \tag{2.4}$$

Integrating from the inner to the outer cylinder we obtain;

$$\Omega_\psi = \int_{R_1}^{R_2} \frac{T\psi\, dr}{2\pi r^3} \tag{2.5}$$

However, if there is any slippage at the cylinder walls, which is considered to occur discontinuously, then the total angular velocity of the rotating cylinder, Ω, is given by;

$$\Omega = \frac{\beta_1 T}{2\pi R_1^3} + \frac{\beta_2 T}{2\pi R_2^3} + \int_{R_1}^{R_2} \frac{T\psi dr}{2\pi r^3} \qquad (2.6)$$

The first two terms in equation 2.6 are the contributions of slippage at the inner and outer surfaces. The third term is the contribution, to the angular velocity, of the material in the gap between the cylinder surfaces. In the limiting case where no slip occurs the first two terms go to zero, since both β_1 and β_2 are zero. The slip coefficient for the different surfaces are given subscripts because different shear stresses occur at the two surfaces, and the slip coefficient is assumed to be only dependent on shearing stress. The concept is shown diagramatically in figure 1.

Using equation 2.6 and different combinations of inner and outer radii it is possible to isolate the angular velocity due to slip and hence the slip coefficients. If the angular velocity, of the rotating cylinder, is measured at constant torque, T, for three combinations of radii namely Ra,Rb;Rb,Rc;Ra,Rc; then combining these measurements the effect of slip may be isolated as below;

$$\Omega_{ab} + \Omega_{bc} - \Omega_{ac} = \frac{T}{2\pi}\left\{ \frac{\beta_a}{R_a^3} + \frac{\beta_b}{R_b^3} + \frac{\beta_b}{R_b^3} + \frac{\beta_c}{R_c^3} - \frac{\beta_a}{R_a^3} - \frac{\beta_c}{R_c^3} + \cdots \right.$$
$$\left. \cdots \int_{R_a}^{R_b} \frac{\psi dr}{r^3} + \int_{R_b}^{R_c} \frac{\psi dr}{r^3} - \int_{R_a}^{R_c} \frac{\psi dr}{r^3} \right\} \qquad (2.7)$$

the right hand side of the above equation reduces to give;

$$\Omega_{ab} + \Omega_{bc} - \Omega_{ac} = \frac{T\beta_b}{\pi R_b{}^3} \tag{2.8}$$

So by measuring the angular velocity of the rotating cylinder, for the three combinations of radii at the same torque, the results may be used to calculate the slip coefficient, β_b. Once the slip coefficient has been determined, as above, the angular velocity due to slip, Ω_β, and fluidity may be calculated from the experimental data.

Since the angular velocity due to fluidity is given by;

$$\Omega_\psi = \int_{R_1}^{R_2} \frac{T\psi dr}{2\pi r^3} \tag{2.5}$$

then transforming r to τ by means of equation 2.3

$$\Omega_\psi = \frac{1}{2} \int_{s_2}^{s_1} \psi d\tau \tag{2.9}$$

In a simple analysis the fluidity function is assumed to be independent of shearing stress in the range s_1 to s_2. As long as the gap is small compared to the overall radii the assumption is approximately true, therefore

$$\Omega_\psi = \psi \frac{(s_1 - s_2)}{2} \tag{2.10}$$

$$\psi s = \frac{\Omega_\psi}{\varepsilon} \tag{2.11}$$

where the right hand side of equation 2.11 equals the shear rate.

Hence, equation 2.11 gives the shear rate dependence of the fluidity function. So far the fluidity function has been considered independent of shear stress across the measuring gap.
However, Mooney (5) proceeds to give a more detailed analysis, in which no assumptions are made as to the dependence of fluidity function on the shearing stress across the gap. This analysis is achieved by expanding the fluidity function as a Taylor series about the mean shear stress. The approach is valid (5) as long as the data shows that the derivatives $d^n\Omega_\psi/ds^n$, to be continuous. Expanding ψ as a Taylor series about the mean shear stress we obtain;

$$\psi = \psi(s) + \frac{d\psi(\tau-s)}{ds\ \ 1!} + \frac{d^2\psi(\tau-s)^2}{ds^2\ 2!} + \ldots + \frac{d^n\psi(\tau-s)^n}{ds^n\ n!} \qquad (2.12)$$

where

$$\frac{d^n\psi}{ds^n} = \left[\frac{d^n\psi}{ds^n}\right]_s$$

by substituting this series into equation 2.9, integrating and introducing the constant ε we obtain an expression for Ω_ψ in terms of ψ and its derivatives.

$$\Omega_\psi = \psi\varepsilon s + \frac{d^2\psi}{ds^2}.\frac{\varepsilon^3 s^3}{3!} + \frac{d^4\psi}{ds^4}.\frac{e^5 s^5}{5!} = \ldots \qquad (2.13)$$

However, we require an expression for ψ in terms of Ω_ψ and its derivatives. This can be achieved by dividing equation 2.13 by s, repeatedly differentiating with respect to s and eliminating the derivatives of ψ from the resulting system of equations;

$$\frac{\Omega_\psi}{s} = u = \psi\varepsilon + \frac{d^2\psi}{ds^2}.\frac{\varepsilon^3 s^2}{3!} + \frac{d^4\psi}{ds^4}.\frac{\varepsilon^5 s^4}{5!} + \ldots \qquad (2.14a)$$

$$\frac{du}{ds} = \frac{d\psi}{ds}\varepsilon + \frac{d^2\psi}{ds^2}.\frac{\varepsilon^3 s}{3} + \frac{d^3\psi}{ds^3}.\frac{\varepsilon^3 s^2}{6} + \ldots \qquad (2.14b)$$

$$\frac{d^2u}{ds^2} = \frac{d^2\psi}{ds^2}\left[\varepsilon + \frac{\varepsilon^3}{3}\right] + \frac{d^3\psi}{ds^3}.\frac{2\varepsilon^3 s}{3} + \ldots \qquad (2.14c)$$

$$\frac{d^3u}{ds^3} = \frac{d^3\psi}{ds^3}\left[\varepsilon + \frac{\varepsilon^3}{3}\right] + \ldots \qquad (2.14d)$$

$$s\psi = \frac{\Omega_\psi}{\varepsilon} - \frac{\varepsilon s}{6 + 2\varepsilon^2}.\frac{d^2u}{ds^2} + \frac{\varepsilon^3 s^2}{9 + 12\varepsilon^2 + 3\varepsilon^4}.\frac{d^3u}{ds^3} + \ldots \qquad (2.15)$$

Equation 2.15 has the desired form. The choice of u, or Ω_ψ/s, means that the first derivative du/ds is not present in the final series. Since ε is generally small, the first term Ω_ψ/ε is usually sufficiently accurate to determine ψ within the limits of experimental error.

2.2 Estimation of the slip layer thickness.

The angular velocities due to slip at the inner and outer surfaces are given by;

$$\Omega_{s1} = \frac{\beta_1 T}{2\pi R_1^2} \tag{2.16}$$

$$\Omega_{s2} = \frac{\beta_2 T}{2\pi R_2^2} \tag{2.17}$$

Assuming that the slip occurs in thin layers of a thickness δ_w, then the mean shear stresses for the inner and outer layers are given by;

$$\tau 1 = \frac{T(R1^2 + (R1 + \delta w)^2)}{4\pi R1^2 (R1 + \delta w)^2} \tag{2.18}$$

$$\tau 2 = \frac{T(R2^2 + (R2 - \delta w)^2)}{4\pi R2^2 (R2 - \delta w)^2)} \tag{2.19}$$

and the corresponding mean shear rates for the inner and outer layers are given by;

$$\gamma 1 = \Omega s1 \frac{(R1^2 + (R1 + \delta w)^2)}{((R1 + \delta w)^2 - R1^2)} \tag{2.20}$$

$$\gamma 2 = \Omega s2 \frac{(R2^2 + (R2 - \delta w)^2)}{(R2^2 - (R2 - \delta w)^2)} \tag{2.21}$$

If we assume that the wall slip layer is a thin layer of water with Newtonian viscosity, then for the inner layer;

$$\eta = \frac{\tau 1}{\gamma 1} = \frac{T}{4\pi\Omega s1} \cdot \frac{(R1^2 + (R1 + \delta w)^2)((R1 + \delta w)^2 - R1^2)}{(R1^2(R1 + \delta w)^2)(R1^2 + (R1 + \delta w)^2)} \qquad (2.22)$$

$$\eta = \frac{T}{4\pi\Omega s1}\left[\frac{1}{R1^2} - \frac{1}{(R1 + \delta w)^2}\right] \qquad (2.22)$$

and rearranging we get;

$$\frac{1}{(R1 + \delta w)^2} = \frac{1}{R1^2} - \frac{4\pi\eta\Omega s1}{T} \qquad (2.23)$$

Similarly for the outer slip layer;

$$\frac{1}{(R2 - \delta w)^2} = \frac{1}{R2^2} + \frac{4\pi\eta\Omega s2}{T} \qquad (2.24)$$

Thus, using equations 2.23 and 2.24, the slip layer thicknesses for the foam may be estimated at any value for the torque at which β, the slip coefficient, has been measured.

2.3.Mathematical descriptions of the flow curves.

Typical flow curves, corrected and uncorrected for slip effects, are shown schematically in figure 2. Attempts to fit commonly used rheological models, such as Bingham plastic and power law (9), to the experimental data have proved unsuccessful. However the uncorrected data can be fitted using a Steiger-Ory model (10);

$$\gamma = a\tau^3 + c\tau \tag{2.25}$$

where; γ = shear rate
τ = shear stress
a,c = constants for the material

However, attempts to fit a modified Steiger-Ory model, with a yield stress included in equation 2.25, to the corrected data were unsuccessful. Two models have been developed that fit the corrected and uncorrected data quite successfully. They have three and four parameters respectively, but have the advantage that estimates of the parameter values can be made from the experimental flow curves. Figure 2 shows how this may be achieved for the two models which are shown below.

Model for Uncorrected data

$$\tau = (\tau_b + \eta\gamma)(1 - \exp^{-\xi\gamma}) \tag{2.26}$$

where; τ = shear stress
γ = shear rate
τ_b = Bingham yield value
η = characteristic viscosity
ξ = "Bingham plastic index"

Model for Corrected data

$$\tau = \tau_y + (\tau_b' + \eta\gamma)(1 - \exp^{-\xi\gamma}) \tag{2.27}$$

Where τ_y is a yield stress, $\tau_b' = \tau_b - \tau_y$ and the constant values are now those applicable to the corrected data.

An estimate of the value of the "Bingham plastic index" may be obtained, for both models from low shear data as follows;

$$e^{-\xi\gamma} = 1 - \xi\gamma + \frac{\xi^2\gamma^2}{2!} - \frac{\xi^3\gamma^3}{3!} + \ldots. \qquad (2.28)$$

at low shear rates equation 2.28 may be reduced to;

$$e^{-\xi\gamma} = 1 - \xi\gamma \qquad (2.29)$$

substituting this result into equation 2.27 gives;

$$\tau = \tau_y + (\tau_b' + \eta\gamma)(1 - 1 + \xi\gamma) \qquad (2.30)$$

rearranging

$$\frac{\tau-\tau_y}{\tau_b'} = \xi\gamma + \frac{\eta\xi\gamma^2}{\tau_b'} \qquad (2.31)$$

$$\frac{\tau-\tau_y}{\tau_b'} \simeq \xi\gamma \qquad (2.32)$$

at low shear rates. As $\gamma < 1s^{-1}$ and τ_b' typically is of the order of 10 Nm^{-2} the second term in equation 2.31 becomes small enough to be ignored.

So, an estimate of the value of ξ can be obtained from the gradient of a plot of the left hand side of equation 2.32 against γ at low shear rates.

As $\xi\gamma$ tends to larger values, $e^{-\xi\gamma}$ approximates to zero and the model can be reduced to a Bingham Plastic, see figure 2. This will occur when the value of $\xi\gamma$ is approximately 5, we can then say that;

SOUTHAMPTON LIBRARY UNIVERSITY

$$\gamma_{limit} \simeq \frac{5}{\xi} \qquad (2.33)$$

Where γ_{limit} is a limiting shear rate below which the behavior of the foam cannot adequately be described by a Bingham Plastic approach.

Once initial estimates of the parameters have been made, from the flow curves as above, they may be optimised using an iterative least squares approach.

3. EXPERIMENTAL APPARATUS AND PROCEDURES.

3.1 Description of foam generation apparatus.

The foam generator consists of a packed bed of glass beads assembled using standard stainless steel tubing and compression fittings. The principle employed is based on an idea published by Patton et.al (2). The device is easily assembled and produces foams of consistent quality (gas volume fraction). The quality may be readily adjusted by varying the volumetric input rates of the gas and liquid.

Nitrogen was used as the filler gas and the foaming liquid was a 1% active solution of a commercially availible alkyl (C_{12}/C_{14}) dimethyl amine oxide in distilled water. The trade name of the surfactant is Empigen OB as supplied by Albright and Wilson Detergents Division, and it is supplied as a 30% active concentrate. This material was chosen as it is a potential candidate for use in enhanced oil recovery processes, 1% active being typical of the concentration which would be considered for such activities. The critical micellar concentration (CMC) for the surfactant was determined as 0.0006 weight percent by du Nouy tensiometry. This CMC value clearly indicates that there will be sufficient availible material for stabilising the foam lamellae, since the working concentration is greatly in excess of the CMC. All of the measurements in this study were performed at an ambient laboratory temperature of 20^{o}c.

A detailed drawing of the generator is shown in figure 3. The liquid phase (aqueous surfactant solution) is injected via a positive displacement metering pump through 0.125" O.D. tube at postion A. It then passes through a bored-out compression fitting (position 1), a snugly fitting guide tube (position 2), and on through a T-junction where the gas stream enters. The guide tube forms a gas tight seal on the liquid tube as the compression fittings are tightened. The liquid tube continues on through a larger diameter tube (position 4), which allows gas to pass around

the outside of the liquid tube and on approximately 0.25" into the packed bed itself.

The bed of glass beads is held in place by glass wool plugs at either end. The inlet gas stream is controlled by a mass flow controller calibrated at atmospheric pressure. This has the advantage of ensuring a constant, atmospheric pressure, foam quality irrespective of variations in the back pressure set up in the foam generator. Once in the bed the liquid and gas phases mix intimately to form a regular foam.

The foam quality produced by the generator can be predicted to within 1% from the following equation;

$$\phi = \frac{V_g \times 100}{(V_l + V_g)} \qquad (3.1)$$

where ϕ = foam quality
V_g = volumetric flow rate of gas (at atmospheric pressure)
V_l = volumetric flow rate of aqueous phase

The system of units used for the flow rates are immaterial as long as they are self consistent.

3.2 Description of the experimental Rheometer.

A major problem in the investigation of the physical properties of aqueous foam is its inherent instability. Foams are thermodynamically unstable systems (1) principally due to their very high surface area compared to their volume. This instability means the foam may well undergo considerable change in structure, due to ageing, whilst measurements are being made. In this study the problem was addressed by adapting a Searle type rheometer so as to allow material to flow through its measuring system. The advantage of the flow-through system is that measurements can be made on "steady state" foam. This is achieved by keeping the flow volume between the foam generator output and the measuring system constant, and maintaining a constant total volumetric flow rate irrespective

of the foam quality required. Such a procedure ensures that the foam contained in the measuring system has always aged to the same extent since its formation. Essentially the experimental data is obtained on "steady state foam". However, this does mean that the foam experiences a shear strain in addition to that induced by the measuring system. This strain is fairly small in magnitude and operates at a right angle to the strain induced by the measuring system. Neglecting this factor may introduce a small error, this however seems a acceptable given that the potentially large effects of foam ageing have been minimized. The rheometer is based on a commercially available instrument (Rotovisco RV100) with the measuring system especially adapted to allow through-flow. The experimental arrangement is shown in figure 4a. The exact positions of the inlet, drainage and extraction tubes were established by visual observation, using a transparent outer cylinder. These were then checked by comparison with flow curves using the more rigid steel cylinder. A detailed chronological account of the observations/adjustments made to obtain the final system arrangement is given in the following paragraphs.

These experiments were performed using a 20mm rotor and a 21mm tube. Two tubes were used, a robust, accurately machined stainless steel tube used subsequently for the measurements, and a perspex tube for visual observations. The latter became slightly warped during manufacture. Initially the foam was fed into the bottom of the measurement system and allowed to overflow the top under its own driving force. The arrangement is illustrated schematically in figure 4b. Using the metal tube, the foam was fed in at 20ml/min and at 80% quality. The foam was subjected to a deformation of $300s^{-1}$ shear continuously in order to check the measurement stability. It was found, from visual observations using the perspex tube, that exceeding this shear rate caused slugging and breakdown of the foam which could be seen in the visual tube. Shearing was started as soon as the foam appeared over the top of the rotor. The measured shear stress seemed fairly stable, although slowly falling, for approximately 15 minutes. After this time the level of the signal

fell dramatically and became very unstable. As the measuring assembly was dismantled a large amount of water was found. This seemed to indicate that draining liquid was building up in the measuring system and causing this instability in the signal level.

The external tube was replaced by the perspex, visual observation, tube and the above sequence repeated. After the 15 minute period liquid build up in the recessed top of the rotor began to overflow, and appeared to cause the shear stress signal to fall dramatically and become unstable. Removing this liquid from the recess with a syringe restored a smooth signal. Furthermore, the overall level of the signal, which had been falling slowly prior to its dramatic demise, was partially restored to its initial value. The remainder of the difference may have been due to a build-up of a water layer on top of the sealing bung at the bottom of the tube. The freshly injected foam had to travel through this layer and was possibly taking up extra water as a result.

The system was reassembled with a bottom drain and a syringe extractor in the rotor recess in an attempt to allieviate the problems encountered above. Re-running the experiment showed a very steady, level signal compared with the previous measurments. The metal tube was substituted for the perspex observation tube and again gave good steady signals.

The next step was to attempt measurements scanning a range of shear rates. The range used was $0\text{-}300s^{-1}$ with a repetitive 2 minute cycle time. The values obtained compared well with those measured at constant shear conditions. The curves although quite smooth showed a slight increase, especially in the low to medium shear rate range. This effect appeared to correspond to banking up of foam in the top of the measuring system. The problem was overcome by installing a vacuum driven extractor as shown in figure 4c.

The cycle time used for the measurement was now investigated. Little effect was noted on the signal in the range 2-10 minutes. Consequently the cycle time was set at 5 minutes, as the lower end of this time scale (2 minutes) was advised against in the literature supplied with the instrument.

The effect of foam delivery rate on the measurements was the next variable to be examined. For an 80% quality foam increasing the delivery rate from 10 to 30 ml/min increased the torque measured by the instrument. However, any subsequent increase in the rate from 30 to 35 ml/min showed no further change. The trend with lower quality foam, 60%, was reversed. The lower delivery rates were now showing higher level torque signals. Generally the 60% foam quality scans also fell with successive cycles. However, the drain in the bottom of the measuring system was only draining liquid at this time. Raising the injector tube to within 0.5" of the inner rotor, and improving the drainage by installing a wider bore drain, removed this time dependence of the torque signal. However, the trend of increasing torque with falling delivery rate, for the 60% quality foam, persisted. This effect was thought to be due to primary liquid drainage from the wet foam leading to a higher signal. Visual observations of the low quality foam showed this primary liquid drainage to be considerable compared to higher quality foams. For a 65% quality foam, the torque signal level still fell with increasing flow rate in the 20-40 ml/min range. However, the flow curves were now grouped much closer together. For a 70% quality foam, curves from 20-40 ml/min were all very similar. Moving to a 75% quality foam showed a reversal of the trend, with the torque signal increasing with delivery rate (20-35 ml/min). Although there was very little difference between the 30 and 35 ml/min signals. For higher quality foams (80,85,90%) this trend persisted. Although again for flow rates in excess of 30 ml/min (ie in the range 30-40 ml/min) there was no appreciable difference in the measured flow curves. Summarising, primary foam degredation seems to weaken the foam structure above 70% foam quality and strengthen it in the lower quality range studied (60-70% quality). The latter effect is probably because of a rise in effective foam quality due to rapid drainage of liquid phase from the foam. However, the former effect is difficult to relate to liquid drainage as visually this does not appear to be a major effect. It may be that at the lower foam delivery rates significant changes in the foam structure occur due

to inter-bubble gas diffusion (Ostwald ripening) (11). Considering the above evidence the decision was taken to restrict the study to foam qualities greater than 70%. Also to standardize on a foam delivery rate of 40 ml/min, reasoning that this would reduce any potential effects due to foam ageing and therefore make comparisons with other work on more stable foam systems, such as fire fighting foams, more valid.

Having derived, within a reasonable time scale, a satisfactory measuring scheme for the work, the rheological study could begin.

3.3 Experimental procedure for the evaluation of wall slip and flow behaviour.

The detailed requirements of Mooney's method (5) for these measurements are given in the theoretical chapter (section 2.1). Presented here is a physical description of the technique as employed for this study. To comply with the mathematical requirements, two measuring tubes and an additional rotor were engineered to the author's design.

The rotors and tubes were used in three combinations;

a) 20mm radius rotor,and 21mm internal radius tube-Gap A

b) 21mm radius rotor,and 22mm internal radius tube-Gap B

c) 20mm radius rotor,and 22mm internal radius tube-Gap C.

To enable the calculation of the slip coefficient, β, angular velocities for the three combinations must be known at equivalent values of the torque. The three results may then be combined to calculate the slip coefficient at that particular torque as disscussed in the theory chapter (section 2.1). This mathematical concept is shown diagrammatically in figure 2. Experimentally the

torque versus angular velocity curves are measured using a programmable controller (the RV100). This controls the angular velocity of the rotor rather than the torque, which is the measured quantity. This problem was over-come by using a computer and plotter with a digitising sight. The digitizing sight is moved over the experimental curves in pre-defined increments of torque. At each value of torque the digitizing sight is positioned on the curve at the value of the angular velocity, corresponding to that torque, is digitized and recorded by the computer software. By using this method, data on the angular velocity at given torque values may be built up and Mooney's method for determining slip coefficients applied. Adjustments were made to the maximum rotor speed on the controller, for each foam quality, to ensure the same range of torque was covered for each measuring system. This procedure enabled the determination of angular velocity at the same given, incremental, torque values for the three different rotor and tube combinations.

The torque versus angular velocity curves used in the digitization process were determined by tracing a smooth curve through the traces obtained by performing at least 10 successive scans of the rotor speed range. This results in "averaged" sets of data on which the slip calculations are based.

3.4. Data processing for the calculation of slip and slip corrected flow curves.

The digitized flow data consist of one hundred individual points. This translates to three hundred data points for each quality foam, requiring a vast amount of calculation. For this reason software was written for the computer system to process the information. Software has been developed to calculate the angular velocities due to slip, and thus the slip coefficients (β). These are then used to calculate flow curves from the data which have the contribution of slip removed. These flow curves are calculated on

the basis of mean shear stress and mean shear rate, assuming that the fluidity is not a function of shear stress over the range present in the measuring gap. This assumption has been validated by comparing these results with a calculation method after Mooney (5), which is given in the theoretical section, based on evaluating the fluidity as a Taylor series . Using this method no a priori assumptions involving the relationship between fluidity and shear stress are required. However, considerable greater calculation is involved, and as comparison showed no discernable differences between the results from the two methods the simpler one was chosen.

3.5 Estimation of Bubble Size in the Foams

An attempt to determine the bubble size was carried out using a glass cell. The cell was constructed from two glass microscope slides sealed with a silicone rubber solution. The slides were separated by strands of fishing line which was 300μm in diameter. The silicone rubber was forced into the gap between the slides using a hypodermic syringe and needle, and allowed to set. This resulted in a seal being formed along the edges of the slides. The assembly was then placed into a mounting block, where holes previously drilled in one of the slides formed seals with 'O' rings present at the ends of flow channels in the block. With this arrangement foam could be pumped into the mounting block and thus between the glass slides.

The complete assembly was then placed onto a laboratory jack below a 35mm camera fitted with bellows and a macro lens for close-up work. Black and white photographs of all the various foam qualities were taken, with the foam allowed to come to rest in the cell. Whilst the work was carried out care was taken not to disturb either the camera or the cell to ensure consistent magnification. To establish the scaling of the photographs the cell was removed from the jack and replaced with a 0.2mm grid marked on plain white paper. The grid was then brought into focus,not by adjusting the camera

assembly but by raising the lab jack. This procedure ensured that the grid was photographed using the same magnification factors as the pictures of the foams. These films were then developed and printed up by the author, again ensuring the magnification was kept constant in the printing process.

The mean bubble diameters were calculated using a form of chord analysis (12), a more detailed analysis was ruled out by the relatively poor quality of the photographs, and also by time constraints. Ten straight lines of a known scaled length were drawn onto a transparent slide, the slide was then placed over a photograph and the number of bubbles intersected by the line counted. From this information the average cord length, z, was calculated as the chord length divided by the average number of bubbles per chord. The average cell diameter, d, is then defined as (12);

$$d = \frac{4z}{\pi} \qquad (3.2)$$

The assumption made here is that the wall thickness is small compared to the bubble width.

It is worth noting at this point the possible causes of error which may result from the sizing technique used. Firstly there is always the possibility that the larger bubbles may be distorted in the 300 μm gap between the glass plates. This would most likely lead to their flattening and cosequent overestimation of their size. Secondly it is difficult to be sure that the sample of foam at the focal plane of the camera, i.e. the surface of the cell, is statistically representative of the bulk foam. Different authors in the literature give differing opinions on this matter. Chang et.al. (13) have reported no significant difference between sizing performed at the surface compared with that performed on a slice through the frozen foam. However, Cheng and Lemlich (14) have suggested that at a wetted surface, which in this case the glass slide is, physical segregation may discriminate against larger bubbles. Also ageing of the foam will result in larger bubbles

growing at the expense of smaller ones, via interbubble gas diffusion (11). Because of these considerations it would be unwise to regard the sizes obtained from this somewhat crude technique as anything more than approximate values.

4.RESULTS AND RHEOLOGICAL DESCRIPTIONS.

4.1 Data uncorrected for wall slip.

The uncorrected flow curves are shown in figures 5a-11a and show the variations obtained for the different measuring systems. There are several points worth highlighting about the flow curves generally. Firstly the overall shape of the curves is similar to that reported in the literature (3,4,15,16,17), although the detailed stress/strain relationships may vary as previously noted (1). These show foam to behave as a pseudoplastic fluid. Furthermore the curves obtained using the 20-22mm measuring system, generally exhibit greater resistance to deformation than for the narrower measuring gaps. This may be explained on the basis of the slip layer and surface area to volume ratio arguments presented in section 5. It is also worth noting the appearance of depressions in the flow curves above 80% foam quality. Apparently as the gas volume fraction in the foam is increasing, the rheological behaviour is becoming more complex.

Attempts to fit a range of rheological models to these flow curves have met with varying degrees of success. Standard descriptions such as those presented by Bingham (9), Ostwald (9), and Casson (18) have proved unsuitable. A fuller description of these fitting exercises is given in appendix 1. The bulk of the main discussion (chapter 5) will concentrate on the phenomenological aspects of the results. However, two descriptions found to give reasonable agreement with the data are shown below:

(i) a pseudoplastic description due to Steiger and Ory (10);

$$\gamma = a\tau^3 + c\tau \qquad (4.1)$$

which defines the flow behaviour with two constants a and c which are typical for the non-Newtonian fluid.

(ii) a three parameter model developed by the author;

$$\tau = (\tau_b + \eta\gamma)(1 - e^{-\xi\gamma}) \qquad (4.2)$$

which has the advantage that the three parameters may be estimated from the raw data as discussed in section 2. Both equations give good fits to the experimental flow curves. However, it should be noted that the constants vary with the geometry of the measuring system as well as with the foam quality. This variation of the apparent viscosity with the geometry of the measuring system has been highlighted by Heller and Kuntamukkula (1).

4.2 Data corrected for slip effects.

The data corrected for wall slip effects are shown in figures 5b-11b. For clarity, the description of these flow curves will be split in two sections. Uncorrected and corrected flow curves for all the foam qualities are shown in figures 19-21 for comparison.

4.2.1 70%-80% foam quality.

The corrected flow curves, for this range of foam qualities, show a much larger degree of coincidence for the various measuring systems than their uncorrected counterparts. With the exception of the 70% quality foam where this improvement is limited to the lower shear range of the measurements. It would appear that correcting for slip at the wall goes a long way towards eliminating the geometric dependence of foam rheology (1). The importance of wall slip in rheological studies of foam has been reported by other authors (3,8,19,20). The curvature of these corrected flow curves is more pronounced and they exhibit a higher resistance to flow (viscosity), than the uncorrected curves. Also, apparent from the corrected curves is the existence of a measurable yield stress, which is in agreement with observations by Wenzel et.al.(21) (on fire fighting foams) and other workers (1,3,15). Below this yield stress the foam will behave very much like a solid. These curves may be adequately described by the 4-parameter equation suggested in section 2

(equation 2.15). The equation in general is in the same form as the three parameter expression (equation 2.14) but with the addition of an extra term to account for the yield stress phenomenon. It has the same advantage in that the parameters can be estimated from the experimental flow curve.

4.2.2 Corrected data 85%-98% foam quality.

The corrected data are no longer smooth in form but are becoming "s" shaped, with the exception of the 98% quality foam. This has a flow curve very similar in form to those of the 70%-80% quality foams. Changes in foam behaviour at around 80% quality have been reported by Calvert et.al. (15). The resistance to deformation (viscosity) is now of the order of more than twice that for the comparable uncorrected curves. The corrected curves are also diverging from the coincidence seen in the lower foam quality range (70%-80%). These curves were originally plotted on the assumption that the fluidity function, ψ, is constant over the shear stress range within the measuring system (5). It is possible that this assumption is failing and causing the divergence in the curves.

Mooney (5) gives a method for calculating flow curves which requires no a priori assumption as to the nature of the relationship between the fluidity function and the shear stress across the gap. The method is based on expanding the fluidity function as a Taylor series about the arithmetic mean shear stress and then integrating. The resultant series from the exercise is as equation 2.15;

$$s\psi = \frac{\Omega_\psi}{\varepsilon} - \frac{\varepsilon s}{6 + 2\varepsilon^2}\frac{d^2u}{ds^2} + \frac{\varepsilon^3 s^2}{9 + 12\varepsilon^2 + 3\varepsilon^4}\frac{d^3u}{ds^3} + \ldots\ldots \qquad (4.3)$$

where, s = mean shear stress

Ω_ψ = angular velocity due to fluidity

$u = \Omega_\psi / s$

$$\varepsilon = \frac{(R_2^2 - R_1^2)}{(R_2^2 + R_1^2)}$$

This equation was applied to the corrected data, numerically calculating the values of the derivatives. This process gave the same resultant curves as applying the simple approximation;

$$s\psi = \frac{\Omega_\psi}{\varepsilon} \qquad (4.4)$$

thus validating the use of the simpler approach for calculating shear rates.

4.3 Estimated thicknesses of the slip layers.

The method used for calculating the slip layer thicknesses is described in section 2, and is similar in form to arguments presented by Thondavadi and Lemlich (8). The slip layer is assumed to be Newtonian with a viscosity equivalent to water (1mPa.s). The variation in the slip layer thickness with shear stress for the different quality foams are shown in figures 12-18a. Generally, the thickness of the layers is in the region of 1-2 μm, this is in agreement with values reported by Kraynik (7) and of the same order of magnitude as those deduced by Thondavadi and Lemlich (8), and has no obvious dependence on the foam bubble size. In the 70%,75% and 80% quality foams the slip layer is approximately 2μm thick at low stress and then tends to thin as the stress is increased. However, the higher quality foams (85%,90%,95%) have a value of around 1.2μm at lower stresses and then tend to thicken as the stress is increased, up to a maximum value around 2μm. With the highest quality foam investigated (98%) the low stress slip layer is approximately 0.9μm across and, although this does thicken with increasing stress the maximum value attained in this study is approximately 1.3μm. This effect of slip layer thickening with increasing shear for foams has also been noted by Thondavadi and

Lemlich (8) in pipe flow with foams of between 88% and 99% quality.

4.4 Estimated Mean Bubble Diameters

Table 1 shows the data obtained from the bubble size analysis described in section 3.5. and figures 22-28 show the pictures taken of the various quality foams. Unfortunately this analysis could not be performed on the 98% quality foam due to the poor picture quality. However, visually it can be seen that the 98% foam falls in with the general trend of increasing bubble size with foam quality. This observation is supported by the work of Thondavadi and Lemlich (8). It is worth noting here that the, pore throat snap off, mechanism of foam formation in glass bead packs observed by Radke and Ramsohoff (22) will mean that the foam morphology will also be highly influenced by the foam generator.

In the opinion of the author the values for bubble sizes given here should only be treated as approximate for the reasons discussed in section 3.5. However, they are given for completeness since one of the criticisms made of many foam rheology studies is the lack of any information as to the bubble size (1).

5. DISCUSSION.

5.1 Yield stress and wall slippage.

There are two important differences between the corrected and uncorrected flow curves (figures 5-11). Firstly, the existence of a measurable yield stress for the foam and, secondly, the much higher resistance to flow compared with the uncorrected curves.

The existence of a yield stress for foam is perhaps not too suprising given its highly structured nature, and the fact that it has been theoretically predicted previously (1,23), for two dimensional model foams. Princen (24) went on to verify experimentally some of his two dimensional model predictions using emulsions. The values of yield stresses found in the present study range from 1.5 to 4 N/m^2, and are shown in table 2, these levels of yield stress are in reasonable agreement with others (15,16,20,25), but below those found by Princen for emulsions (24). For the 70%, 75%, and 80% foam qualities the yield stress shows an upward trend, but this does not extend to the higher quality foams where no discernible trends exist. The most important consequence is that the yield stress must be exceeded before shear flow can be established in the bulk foam. Any flow occuring prior to this must be attributable to wall slippage. Heller and Kuntamukkula (1) used these considerations as the basis for a method to determine the slip layer thickness in pipe flow. Experimental work presented by Kraynik (7), and Thondavadi (8) indicates this slip layer to be of the order of a few microns, in agreement with the values found in this study. This contrasts with Calvert (15), who estimates slip layer thicknesses in the region of 20-70 microns, based on a curve fitting approach. The width of the slip layer will have a profound effect on the flow behaviour of foam. Wall slip may go a long way towards explaining the variation of flow behaviour with flow geometry found both here and in the literature (1).

Figures 12-18 show the variation in slip layer thickness with shear stress contrasted with the rheograms for the foam itself (nb

in these figures the rheograms are plotted the opposite way round to figures 5b-11b for ease of comparison). When combined these two effects give rise to the original uncorrected flow curves. It is important to appreciate that the observed flow behaviour of foam is a net result of the interplay of these two effects.

Heller and Kuntamukkula (1) give a method for calculating the bubble wall thickness, Δr, and the maximum slip layer thickness, $(\delta_w)_{max}$, for an idealised monodisperse foam,

$$\Delta r = r_b(1 - \phi^{1/3}) \tag{5.1}$$

$$(\delta_w)_{max} = \pi[r_b(1 - \phi^{1/3}) - t_c] \tag{5.2}$$

here t_c is the critical bubble wall thickness prior to rupture and is taken as 0.1 μm. Although not strictly applicable to real polydisperse foams, these equations may be used to estimate whether there is sufficient supply of liquid available to produce the slip layers, without the collapse of bubbles. Table 3 shows the results of these calculations for the foams used in the present study, and confirm the quoted slip layer thicknesses are within these limits.

5.2 Variations in slip layer thicknesses for the various foam qualities.

The variations of slip layer thickness are complex and for clarity the discussion will be divided into two sections. For the purpose of this discussion bulk foam will refer to deformation in the body of the foam excluding the slip layers.

5.2.1 70%, 75%, and 80% foam quality.

Generally once flow has been established in the bulk foam ($\simeq$20 s^{-1}) the slip layers begin to thin, and the bulk foam becomes increasingly shear thinning. This thinning of the slip layers may be a result of the adjacent bubbles being forced into the layers as

they attempt to move past their counterparts. At high stress (≈15 Pa) in the 70% foam there appears to be an almost catastrophic failure of the slip layer. It could be that the imposition of further stress would result in bubbles beginning to rupture at the walls, as the critical bubble wall thickness is approached. This may herald the onset of shear destruction of the prevailing foam structure.

5.2.2 85%, 90%, 95%, and 98% foam quality

In the case of these higher quality foams, the above behaviour seems to be reversed. As flow is established in the bulk foam further strain appears to squeeze water from the foam structure, into the slip layers causing them to thicken. This behaviour has been observed previously (8) for foams of qualities in the 88% to 99% range. The degree of structuring in foam will increase with gas volume fraction and start to become acute at 74% (the ideal packing fraction for monodiperse spheres), with polydispersity this value may be higher (1,15), and experimentally (15) has been found to be about 80%. These more highly structured foams will have a much greater resistance to flow deformation. It is possible that as the foam cells are being forced past each other, the resulting stresses may force water out of the foam lamellae, causing it to migrate to the edges of the flow system and into the slip layers. Thickening of the slip layers will permit more dissipation of strain at the edges of the flow system, thus reducing the requirement for the bulk foam to deform. The stress at which the slip layers begin to thicken increases with foam quality. It appears that as the foam lamellae are becoming thinner, greater stresses are required to squeeze water from them. This is reflected in the flow curve of the bulk foam. In the flow curves of the 85%, 90%, and 95% bulk foams, there exists a region where additional stress results entirely in thickening of the slip layers. In this region there is no further strain taken up by the bulk foam. However, with the 98% bulk foam no such region exists.

It is worth noting that with the higher quality foams, i.e. 85% and greater, that the number of bubbles across the rheometer gap is typically less than 10 and 5, for the measuring sytems used. More work is needed, using larger measuring devices or smaller bubble foams, to confirm whether this redistribution of water under shear is a general property of bulk foam, or peculiar to foam flow in confined geometries.

5.3 Discussion of flow curves corrected for wall slip.

The corrected flow curves for bulk foam generally show a much greater resistance to deformation (i.e. a much higher viscosity) than would be supposed from the raw data (figures 5-11). Consequently data for foam flow gathered from laboratory rheometers could be in serious error when applied to other situations, industrial plants for example. These implications are discussed more fully in section 5.4.

For the lower quality foams (70%, 75%, and 80%) the corrected curves show a large degree of coincidence, compared to the raw data. These curves may be considered to represent the true rheological characteristics of the bulk foam. They show the foam to be plastic in nature, possessing a yield stress. The above comments are also true of the 98% quality bulk foam.

However, in the case of the 85%, 90%, and 95% quality bulk foam the corrected flow curves are no longer simple in nature. The 90% and 95% flow curves, in particular show a marked degree of divergence. An explanation for the unusual shape of these rheograms has been proposed in the previous section, on the basis of redistribution of the water in the foam structure. The divergence in the mean shear rates for the various measuring gaps does show a pattern. The lowest shear rates always pertain to the 21-22mm gap (ie. the outer one), the 20-21mm gap (ie. the inner one) always gives the highest values, and the medium values occur for the 20-22mm gap (which encompasses the other two). If the results may be

attributed to any physical reality, an idea given some credence by the Taylor analysis presented in section 4.2.2, then it may be that the shear rate in the bulk foam is falling rapidly across the measuring gaps. It could be that the foam structure is deforming, so as to allow flow, in a manner analogous to the 2-dimensional descriptions proposed by Kraynik and Hansen (26). These descriptions allow for foam flow by deformation of the hexagonal cells into parallelograms, which may then slide past each other more easily. The net result of such a flow regime in the concentric cylinder geometry used here, would be the flow of concentric layers of foam cells around each other as shown in figure 29. Much of the flow would tend to occur in the water layers between the cells, which could be regarded as slip layers within the foam structure. In this type of flow regime the strain would be dissipated in a stepwise manner across the measuring gap, as illustrated in figure 29. This rationale of foam flow obviously requires more weighty scientific evidence to support it. However it is presented here with the aim of stimulating future work and discussion.

5.4 Implications for flow calculations.

This work has shown the contribution of wall slip effects in the measurement of foam flow properties to be very significant. The same may be true of other two phase systems with a high disperse volume fraction, for example slurries, pastes, and emulsions. Given that the dispersed phase in these systems could be considered incompressible compared to the gas phase in foams, such systems might be expected to show even greater yield stresses and hence resistance to flow. Therefore the effects discussed here for foams, may be even more pronounced in these types of dipersions. If wall slip exists in such a system, then using measurements from laboratory rheometers to estimate flow characteristics in other environments, such as industrial plants and pipelines for example, could result in serious errors. These errors would be largely due to variations in the surface area to volume ratios between the

laboratory and other flow geometries. The larger the value of the surface area to volume ratio the greater the effect wall slip will have on the observed flow behaviour. A far more accurate approach to such calculations would be to determine the bulk flow properties of the system and the thickness of the slip layer. Then calculations of the flow characteristics may be made by individually assessing the two effects and then combining these to give a final answer.

In the absence of such data for the flow system, it is the opinion of the author that calculations should be made assuming minimum and maximum wall layer thicknesses, to check against the no slip calculations. It is suggested that the values to adopt would be 1μm and 10μm respectively, if the results differ wildly from the no slip case then further experimental work would seem to be required.

6.CONCLUSIONS.

6.1 The method of Mooney (5,6) for determining slip effects in a concentric cylinder rheometer have been applied to foams in this study. The method appears to work well, and the corrections applied go some way to reducing dependence of the observed flow properties on the geometry on the measuring system used.

6.2 The wall slip layer thicknesses found for foam are generally between 1 and 3μm and appear to be well under the calculated maxima after a method proposed by Heller and Kuntamukkula (1). The thickness of the slip layers appears to be influenced by foam quality, bubble size and the applied shear field acting on the foam.

6.3 This study of foam rheology over a range of foam qualities (70-98%) has shown the significant contribution wall slip effects may have on the measurements. If these slip effects are ignored the flow properties deduced from the study may be in serious error.

6.4 When slip effects are taken into account and corrected for, the flow resistance (viscosity) of the bulk foam is considerably higher than is immediately apparent from the laboratory results.

6.5 The corrected flow properties confirm the existence of a yield stress for foam in accordance with theoretical predictions (1,23) and experimental observations (15,16,20,25) made by other workers. Generally the yield stress is of the order of a few N/m^2, but no good correlation was observed with foam quality.

6.6 The overall flow behaviour of foam results from a complex interplay of flow in slip layers at the edges of the system, and flow of the bulk foam structure itself. Published work (1) has identified the variations in observed foam flow properties reported

by different authors. The neglect of slip layer effects is probably a major cause of many of these inconsistencies. In the calculation of foam flow properties in real situations (e.g. pipelines, wellbores etc.) it will be important to attempt to allow for wall slip effects. This consideration will be particulary important when scaling up laboratory foam flow data to industrial plant. The large differences in the wall surface area to volume ratios of the laboratory and plant could lead to serious errors in calculated pressure drops and flow rates.

7. SUGGESTIONS FOR FUTURE WORK.

This study of foam rheology has identified wall slip as an important factor in the flow of foam as measured in a concentric cylinder rheometer, and is in agreement with the findings of other workers for pipes (1,8). It would be interesting to investigate this phenomenon using more complicated geometries, for example variable diameter tubes or valves to assess whether the effect is still as important.

It has been suggested herein that with high quality foam (85-95%), that water may be squeezed out of the structure under the influence of applied stress so as to lead to a thickening of the wall slip layers. However, this effect seems to be largely negated at very high foam quality (98%), possibly due to the lack of available 'free' water. By changing the mobility of water in the foam using additives in the aqueous phase, valuable insight may be gained allowing the phenomenon to be better understood by performing similar rheological measurements to those in this work. For example, adding polymers to the aqueous phase will increase its viscosity, and as a consequence squeezing water from the foam structure may become less favourable. Comparing similar foam systems with and without polymer present could yield some interesting results.

In very high quality foams where the bubble lamellae are becoming very thin, the water may be prevented from migrating to the slip layers by the double layer forces present at the lamellae surfaces. The two ionic atmospheres present at each surface may impinge upon each other preventing further thinning via electrostatic repulsion. The effective range of the ionic atmosphere extending from the surface will be reduced (27) by adding salt to the foaming solution. This may allow more water to be squeezed from the foam films. Comparing the rheology of high quality foams, with and without added salt, may well reveal some interesting aspects regarding this redistribution of water in the foam structure.

It has been speculated on the basis of this work that real

foam may actually flow in a way akin to that proposed from two dimensional modelling published by others (26). An investigation of local velocities in flowing foam could provide valuable insight regarding these ideas, and their applicability to real polydisperse three-dimensional foams.

8.REFERENCES.

(1) Critical Review of the Foam Rheology Literature
J.P.Heller and M.S.Kuntamukkula
Ind.Eng.Chem.Res 1987, 26, pg 318

(2) The Rheology of Mobility Control Foams
J.T.Patton, S.J.Holbrook and W.Hsu
Society of Petroleum Engineers Journal June 1983 pg 456

(3) The Rheology of Foam
A.David and S.S.Marsden
Society of Petroleum Engineers paper 2544 Oct 1969

(4) Mechanisms of Foam Flow in Porous Media-Apparent Viscosity in Smooth Capillaries
G.J.Hirasaki and J.B.Lawson
Society of Petroleum Engineers paper 12129 Oct 1983

(5) Explict Formulas for Slip and Fluidity.
M.Mooney
Journal of Rheology, April 1931 pg 210

(6) Wall Slip Corrections for Capillary, Couette, and Parallel Disk Viscometers
A.Yoshimura and R.K.Prud'homme
Society of Petroleum Engineers paper 14696 March 1985

(7) A.M.Kraynik-Abstract of Presentation
Presented at the Annual Meeting of the Society of Rheology, Evanston IL Oct 24-28 1982 Paper B10

(8) Flow Properties of Foam With and Without Solid Particles
N.N.Thondavadi and R.Lemlich
Ind.Eng.Chem.Process Des.Dev. 1985,24,748-53

(9) Viscosity and Flow Measurement
J.R.van Wazer, J.W.Lyons, K.Y.Kim and R.E.Colwell
Interscience Publishers, John Wiley and Sons 1963

(10) Interpretation of Flow Curves
K.Steiger-Trippi and A.Ory
Pharm.Acta.Helv. 1961 Vol 36 pg 205

(11) An Equation Describing Aqueous and Non-aqueous Foam Collapse
I.C.Callaghan, Lawrence F.T. and Melton P.M.
Colloid and Polymer Science. 264: pg 423 (1986)

(12) Low Surface Energy Polymers and Surface-Active Block Polymers
II.Rigid Microporous Foams by Emulsion Polymerization
M.H.Litt, B.R.Hsieh, I.M.Krieger, T.T.Chen, and H.L.Lu
J.Colloid and Interface Sci. Vol.115 No.2 Feb.1987

(13) Bubble Size and Bubble Size Determination
R.C.Chang, H.M.Schoen and C.S.Grove
Ind.Eng.Chem. 1956, 48, 2035

(14) Errors in the Measurement of Bubble Size Distributions in Foam
H.C.Cheng and R.Lemlich
Ind.Eng.Chem.Fundam. 1983, 22, 105-109

(15) A Rheological Model of a Liquid-Gas Foam
J.R.Calvert and K.Nezhati
Int.J.Heat and Fluid Flow Vol 7 No 3 Sept 1986 pg 164

(16) Rheology of Foam and its Implications in Drilling and Cleanout Operations
V.Sanghani and C.U.Ikoku
United States Dept.Eng Report. DOE/BC/10079-47 DE82 015399

(17) The Flow of Foam Through Short Porous Media and Apparent Viscosity Measurements
S.S.Marsden and S.A.Khan
Society of Petroleum Engineers Journal March 1966 pg 17

(18) Introduction to Practical Viscometry
G.Schramm
Haake Gmbh 1981

(19) Flow of High Expansion Foam in Pipes
H.G.Wenzel, T.E.Stelson and R.J.Brungraber
J.Eng.Mech.Proc.of ASCE Dec.1967 6,153

(20) Flow Behaviour of Foam as a Well Circulating Fluid
A.H.Beyer, R.S.Millhone and R.W.Foote
Society of Petroleum Engineers paper 3986 Oct.1972

(21) The Viscosity of High Expansion Foam
H.G.Wenzel, R.J.Brungraber and T.E Stelson
J.Materials, JMLSA, vol 5 no 2 June 1970 pg 369

(22) Mechanisims of Foam Generation in Glass Bead Packs
C.J.Radke and T.C.Ramsohoff
Society of Petroleum Engineers paper 15441 Oct 1986

(23) Rheology of Foams and Highly Concentrated Emulsions 1.Elastic Properties and Yield Stress of a Cylindrical Model System
H.M.Princen
J.Colloid and Interface Sci. Vol 91,No 1, Jan 1983 pg 160

(24) Rheology of Foams and Highly Concentrated Emulsions. II Experimental Study of the Yield Stress and Wall Effects for Concentrated Oil-in-Water Emulsions
H.M.Princen
J.Colloid and Interface Sci. Vol 105,No.1, May 1985 pg 150

(25) Foam Rheology: III Measurement of Shear Flow Properties
S.A.Khan, C.A.Schnepper, and R.C.Armstrong
Journal of Rheology 32(1),69-92 (1988)

(26) Foam Rheology: A Model of Viscous Phenomena
A.M.Kraynik and M.G.Hansen
Journal of Rheology 31(0),175-205 (1987)

(27) Physical Chemistry
W.J.Moore
Prentice-Hall Inc. New Jersey 1972 Ed.5 pg 453

9.1 Appendix 1. Curve Fitting to the Flow Curves.

The shape of the uncorrected flow curves indicate foam to behave as a psuedoplastic fluid, this is in agreement with the findings of others (3,7,8). These flow curves may be described by the Steiger-Ory or three parameter equations as outlined in section 2.3.

$$\gamma = a\tau^3 + c\tau \qquad \text{(Steiger-Ory)}$$

$$\tau = (\tau_b + \eta\gamma)(1 - e^{-\xi\gamma}) \qquad \text{(3 parameter equation)}$$

The values of the constants (τ_B, η, ξ), in the three parameter model, are listed in table 5. They show no obvious trend with varying foam quality. However, the values of all three constants show a marked change between 80% and 90% foam quality, and indeed the value of η for the 85% quality foam in the 20-22mm measuring system is negative. Generally the values of η and ξ for the 20-22mm measuring system are notably higher than for the two narrower measurement systems. This is indicative of an increasing resistance to deformation which is apparent from the flow curves.

The constants from the Steiger-Ory descriptions of the uncorrected flow curves are shown in table 4. The logarithm of the cubic parameter, a, shows a decrease with the gas volume fraction, but varies for the different measuring gaps. This parameter controls the severity of the curvature present in the flow curve, and indicates that the higher quality foams tend towards a more Newtonian, apparent behaviour. The values of the second parameter, c, show considerable variation both with quality and measuring gap.

Although both these equations fit the uncorrected experimental data reasonably well (see figure 30) neither show any good correlations with varying foam quality. This severely restricts their value as predictive equations, and the variation of the parameters with the measuring gaps only serves to emphasize the geometry dependence of foam rheology previously mentioned.

The four-parameter equation developed to fit the data corrected for wall slip is only applicable to the 70, 75 and 80% foam qualities. The values of the parameters are given in table 6, and examples of the fitted curves are shown in figure 31. For a given foam quality one curve gives a reasonable fit to the data for all three measuring gaps. However, only being applicable over such a restricted range of foam quality minimizes its usefulness.

For the sake of completeness, and in case other workers may wish to make use of these equations the least squares method used to fit the three and four-parameter curves is presented here.

9.2 CURVE FITTING THE THREE PARAMETER MODEL FOR FOAM FLOW.

The equation to be fitted is as follows,

$$\tau_i = (\tau_b + \eta\gamma_i)(1 - e^{-\xi\gamma_i}) \qquad (A.1)$$

so at any given experimental point

$$\tau_i = f(\tau_b, \eta, \xi) \qquad (A.2)$$

If the values of τ_b, η, and ξ are estimated the resulting calculated values of τ_i will differ from the experimental value by;

$$\tau_{i(calc)} - \tau_{i(expt)} = \Delta\tau_i \qquad (A.3)$$

$$\Delta\tau_i = \left(\frac{d\tau_i}{d\tau_b}\right)\Delta\tau_b + \left(\frac{d\tau_i}{d\eta}\right)\Delta\eta + \left(\frac{d\tau_i}{d\xi}\right)\Delta\xi \qquad (A.4)$$

where $\Delta\tau = \Delta\tau_{b(estimated)} - \tau_{b(true)}$, similarly for $\Delta\eta$ and $\Delta\xi$ rewriting

$$\Delta\tau_i = a\Delta\tau_b + b\Delta\eta + c\Delta\xi \qquad (A.5)$$

where,

$$a = \frac{d\tau_i}{d\tau_b} = 1 - e^{-\xi\gamma_i} \qquad b = \frac{d\tau_i}{d\eta} = \gamma_i - \gamma e^{-\xi\gamma_i}$$

$$c = \frac{d\tau_i}{d\xi} = \tau_b\gamma_i e^{-\xi\gamma_i} + \eta\gamma_i^2 e^{-\xi\gamma_i}$$

the values of $\Delta\tau_b$, $\Delta\eta$, and $\Delta\xi$ which best satisfy equation A.5 are given when S is a mininmum,

$$S = \sum_{i=1}^{n} (\Delta\tau_i - a\Delta\tau_b - b\Delta\eta - c\Delta\xi)^2 \qquad (A.6)$$

this is achieved when

$$\frac{dS}{d\Delta\tau_b} = \frac{dS}{d\Delta\eta} = \frac{dS}{d\Delta\xi} = 0 \qquad (A.7)$$

we may now generate a set of three equations in the errors of the estimated fitting parameters $\Delta\tau_b$, $\Delta\eta$ and $\Delta\xi$;

$$\Delta\tau_b\Sigma a^2 + \Delta\eta\Sigma ab + \Delta\xi\Sigma ac \_ \Sigma a\Delta\tau_i = 0 \qquad (A.8)$$

$$\Delta\tau_b\Sigma ab + \Delta\eta\Sigma b^2 + \Delta\xi\Sigma bc \_ \Sigma b\Delta\tau_i = 0 \qquad (A.9)$$

$$\Delta\tau_b\Sigma ac + \Delta\eta\Sigma bc + \Delta\xi\Sigma c^2 - \Sigma c\Delta\tau_i = 0 \qquad (A.10)$$

these equations may be solved using a matrix method ($\tau=\Delta\tau_i$);

$$\frac{\Delta\tau_b}{\begin{vmatrix} \Sigma ab & \Sigma ac & -\Sigma a\tau \\ \Sigma b^2 & \Sigma bc & -\Sigma b\tau \\ \Sigma bc & \Sigma c^2 & -\Sigma c\tau \end{vmatrix}} = \frac{-\Delta\eta}{\begin{vmatrix} \Sigma a^2 & \Sigma ac & -\Sigma a\tau \\ \Sigma ab & \Sigma bc & -\Sigma b\tau \\ \Sigma ac & \Sigma c^2 & -\Sigma c\tau \end{vmatrix}} = \frac{\Delta\xi}{\begin{vmatrix} \Sigma a^2 & \Sigma ab & -\Sigma a\tau \\ \Sigma ab & \Sigma b^2 & -\Sigma b\tau \\ \Sigma ac & \Sigma bc & -\Sigma c\tau \end{vmatrix}} =$$

$$= \frac{-1}{\begin{vmatrix} \Sigma a^2 & \Sigma ab & \Sigma ac \\ \Sigma ab & \Sigma b^2 & \Sigma bc \\ \Sigma ac & \Sigma bc & \Sigma c^2 \end{vmatrix}}$$

rewriting

$$\frac{\Delta\tau_b}{|\tau_b|} = \frac{-\Delta\eta}{|\eta|} = \frac{\Delta\xi}{|\xi|} = \frac{-1}{|D|} \qquad (A.11)$$

where

$$|\tau_b| = \Sigma ab(\Sigma b\tau \Sigma c_2 - \Sigma bc \Sigma c\tau) - \Sigma ac(\Sigma b\tau \Sigma bc - \Sigma b2 \Sigma c\tau) - \Sigma a\tau(\Sigma b2 \Sigma c2 - \Sigma bc \Sigma bc)$$

$$|\eta| = \Sigma a^2(\Sigma b\tau \Sigma c^2 - \Sigma bc \Sigma c\tau) - \Sigma ac(\Sigma b\tau \Sigma ac - \Sigma ab \Sigma c\tau) - \Sigma a\tau(\Sigma ab \Sigma c^2 - \Sigma bc \Sigma ac)$$

$$|\xi| = \Sigma a^2(\Sigma b\tau \Sigma bc - \Sigma c\tau \Sigma b^2) - \Sigma ab(\Sigma b\tau \Sigma ac - \Sigma c\tau \Sigma ab) - \Sigma a\tau(\Sigma ab \Sigma bc - \Sigma b^2 \Sigma ac)$$

$$|D| = \Sigma a^2(\Sigma b^2 \Sigma c^2 - \Sigma bc \Sigma bc) - \Sigma ab(\Sigma ab \Sigma c^2 - \Sigma bc \Sigma ac) + \Sigma ac(\Sigma ab \Sigma bc - \Sigma b^2 \Sigma ac)$$

So we may now calculate the errors in the original estimates of the equation parameters, and by an iterative process arrive at the best possible values to fit the experimental data.

9.3 CURVE FITTING THE FOUR PARAMETER MODEL FOR FOAM FLOW.

The equation to be fitted is as follows,

$$\tau_i = \tau_y + (\tau_b' + \eta\gamma_i)(1 - e^{-\xi\gamma_i}) \qquad (A.12)$$

so at any given experimental point

$$\tau_i = f(\tau_y, \tau_b', \eta, \xi) \qquad (A.13)$$

If the values of τ_y, τ_b', η, and ξ are estimated the resulting calculated values of τ_i will differ from the experimental values by;

$$\Delta\tau_i = \tau_{i(calc)} - \tau_{i(expt)} \qquad (A.14)$$

$$\Delta\tau_i = \left[\frac{\delta\tau_i}{\delta\tau_y}\right]\Delta\tau_y + \left[\frac{\delta\tau_i}{\delta\tau_b}\right]\Delta\tau_b + \left[\frac{\delta\tau_i}{\delta\eta}\right]\Delta\eta + \left[\frac{\delta\tau_i}{\delta\xi}\right]\Delta\xi \qquad (A.15)$$

where $\Delta\tau_y = \tau_{y(estimated)} - \tau_{y(true)}$, similarly for $\Delta\tau_b$, $\Delta\eta$, and $\Delta\xi$ rewriting equation A.15

$$\Delta\tau_i = a\Delta\tau_y + b\Delta\tau_b + c\Delta\eta + d\Delta\xi \qquad (A.16)$$

the values of $\Delta\tau_y$, $\Delta\tau_b$, $\Delta\eta$, and $\Delta\xi$ which best satisfy equation A.16 are those which give the following summation, S, as a minimum;

$$S = \sum_{i=1}^{n}(\Delta\tau_i - a\Delta\tau_y - b\Delta\tau_b - c\Delta\eta - d\Delta\xi)^2 \qquad (A.17)$$

this condition is satisfied when,

$$\frac{dS}{d\Delta\tau_y} = \frac{dS}{d\Delta\tau_b} = \frac{dS}{d\Delta\eta} = \frac{dS}{d\Delta\xi} = 0 \qquad (A.18)$$

the resultant system of equations to be solved is

$$\Delta\tau_y\Sigma a^2 + \Delta\tau_b\Sigma ab + \Delta\eta\Sigma ac + \Delta\xi\Sigma ad - \Sigma a\Delta\tau_i = 0 \qquad (A.19)$$

$$\Delta\tau_y\Sigma ab + \Delta\tau_b\Sigma b^2 + \Delta\eta\Sigma bc + \Delta\xi\Sigma bd - \Sigma b\Delta\tau_i = 0 \qquad (A.20)$$

$$\Delta\tau_y\Sigma ac + \Delta\tau_b\Sigma bc + \Delta\eta\Sigma c^2 + \Delta\xi\Sigma cd - \Sigma c\Delta\tau_i = 0 \qquad (A.21)$$

$$\Sigma\tau_y\Sigma ad + \Delta\tau_b\Sigma bd + \Delta\eta\Sigma cd + \Delta\xi\Sigma d^2 - \Sigma d\Delta\tau_i = 0 \qquad (A.22)$$

The system of equations is solved via the matrix method used for the 3-parameter equation and the corrections ($\Delta\tau_y$ etc.) to the initial estimated values are calculated. The corrected estimates are then fed back into the process to produce further corrections, this iterative process is repeated until a satisfactory curve fit is obtained.

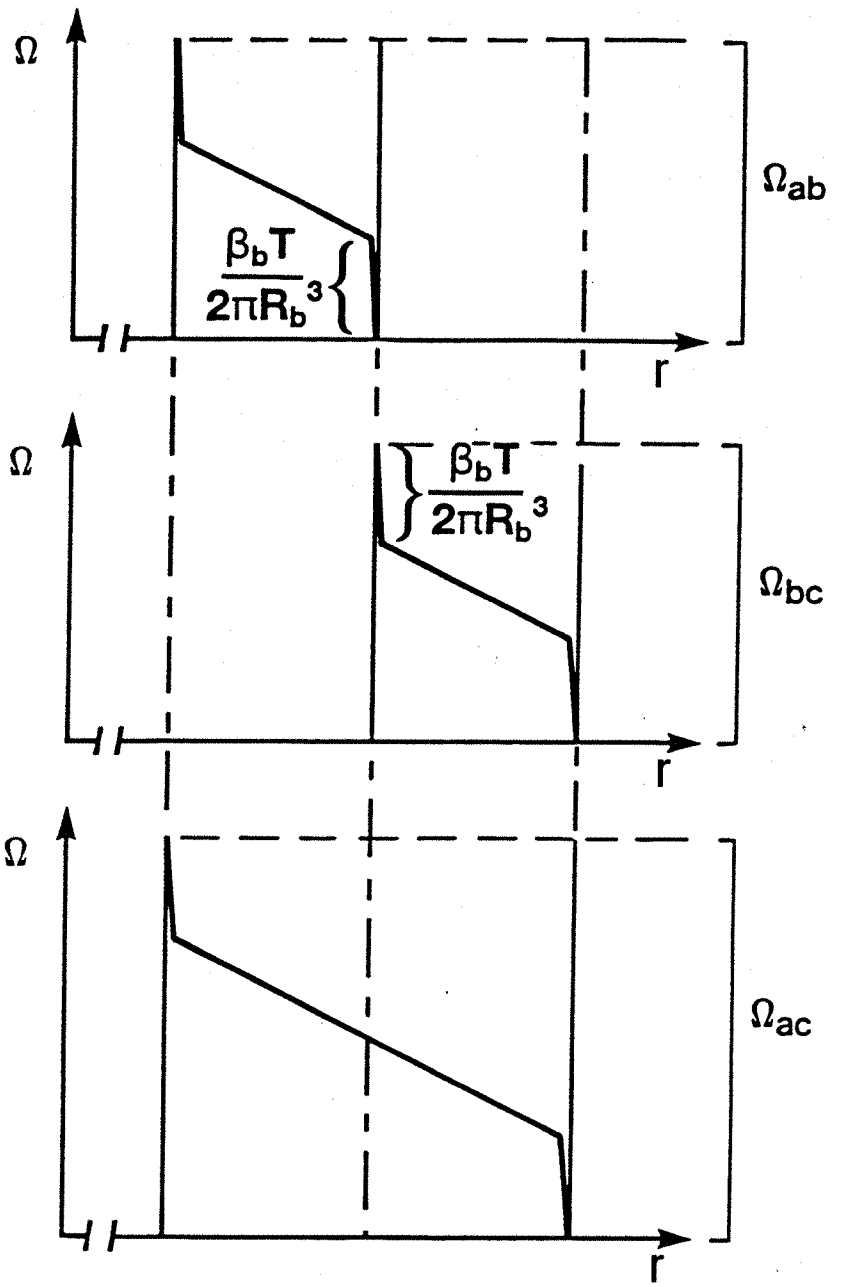

FIGURE 1:

Diagramatic representation of slip measurements:

$$\Omega_{ab} + \Omega_{bc} - \Omega_{ac} = \frac{\beta_b T}{\pi R_b^3}$$

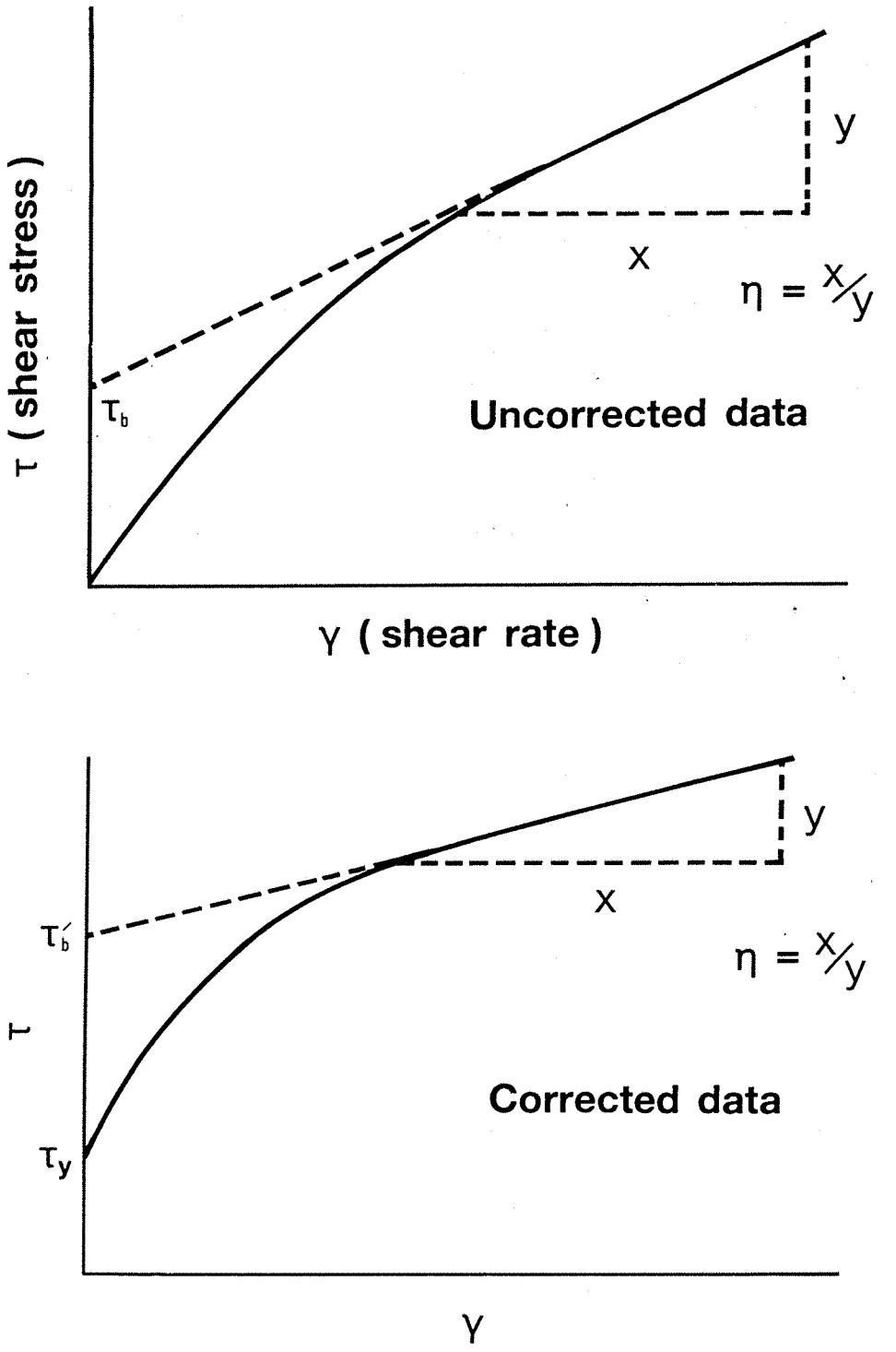

FIGURE 2;
Schematic of corrected and uncorrected flow curves.

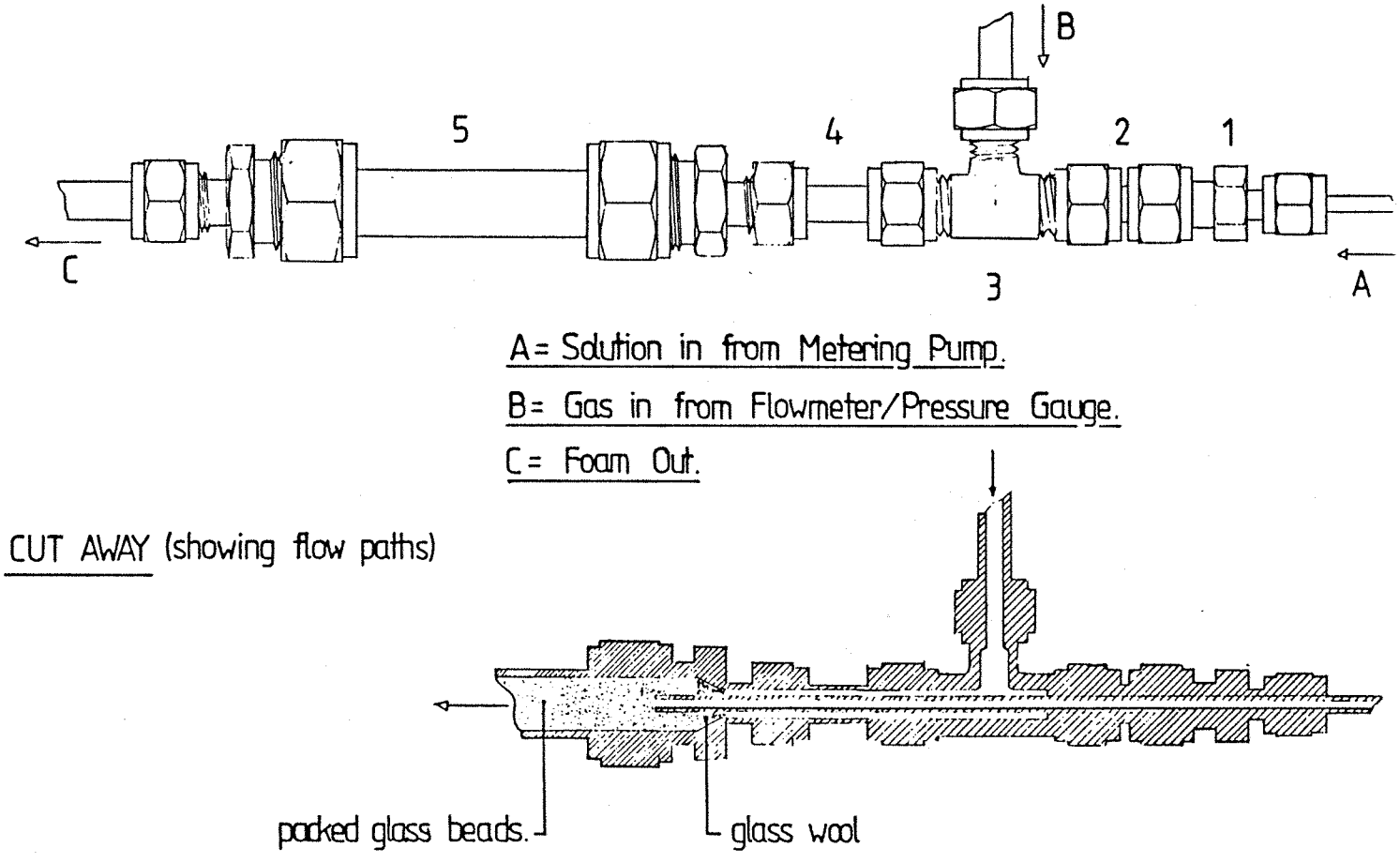

Figure 3.

Packed Bed Foam Generator (½ scale)

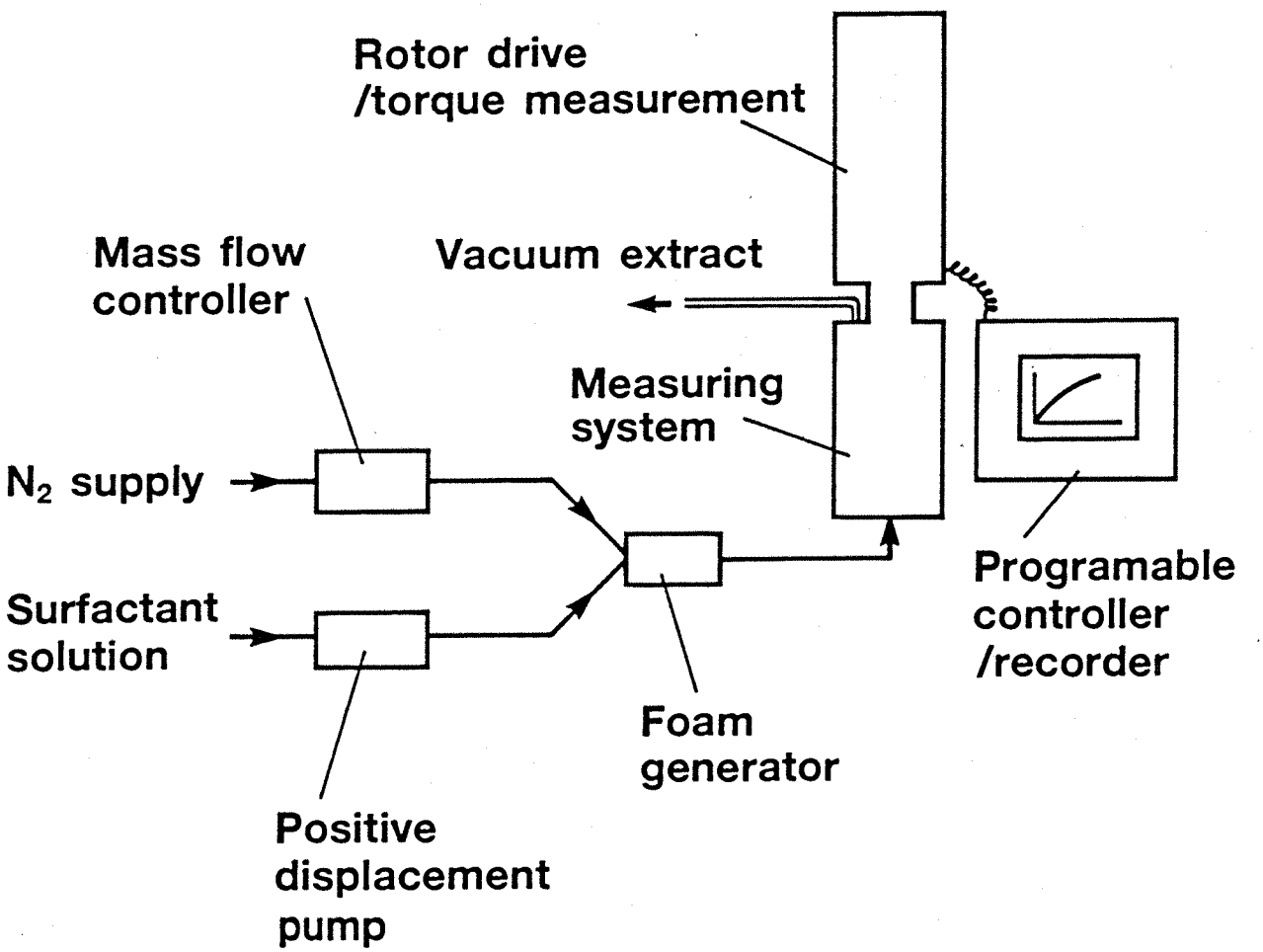

Figure 4a Schematic of apparatus.

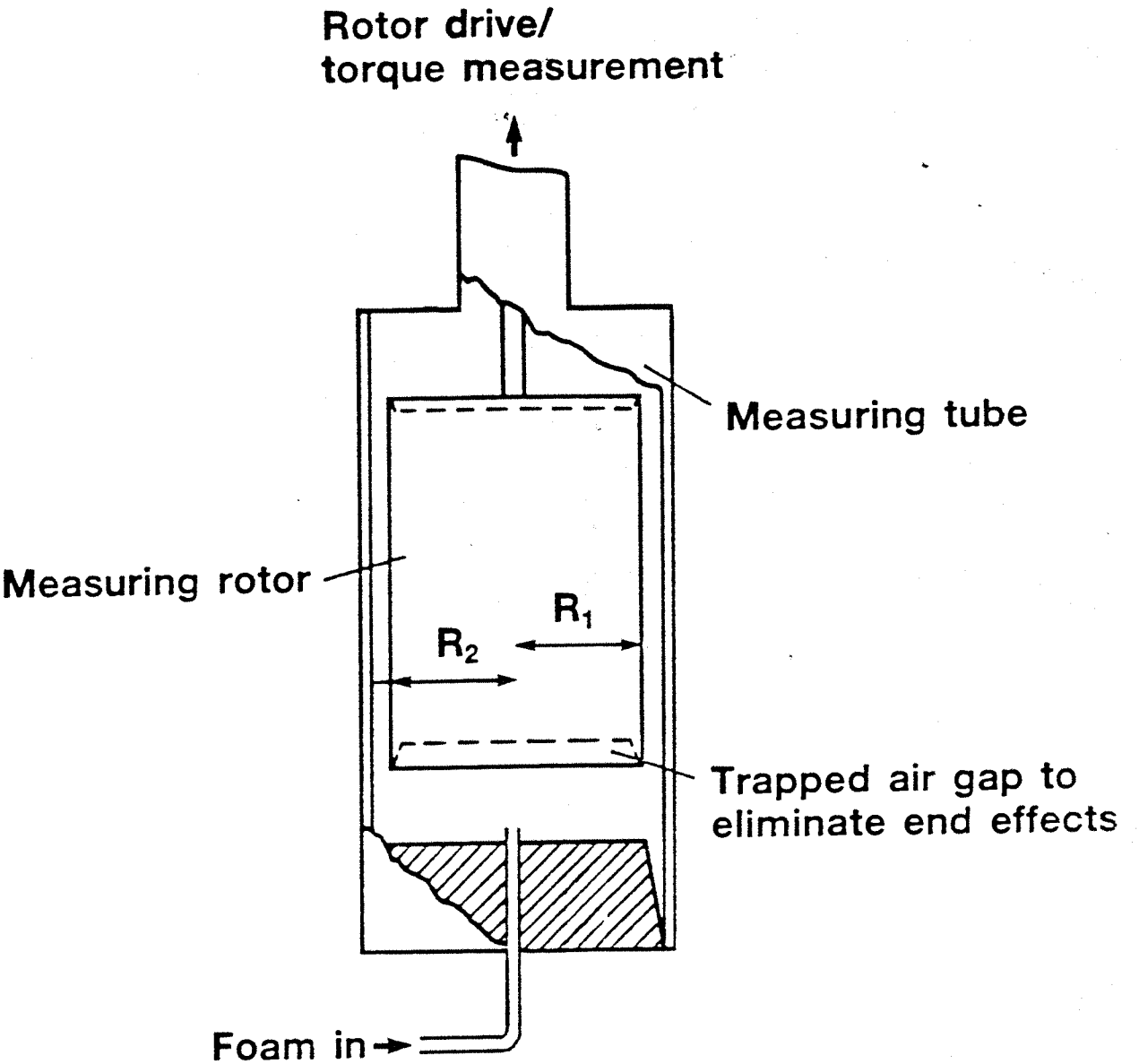

Figure4b Exploded view of measuring system.

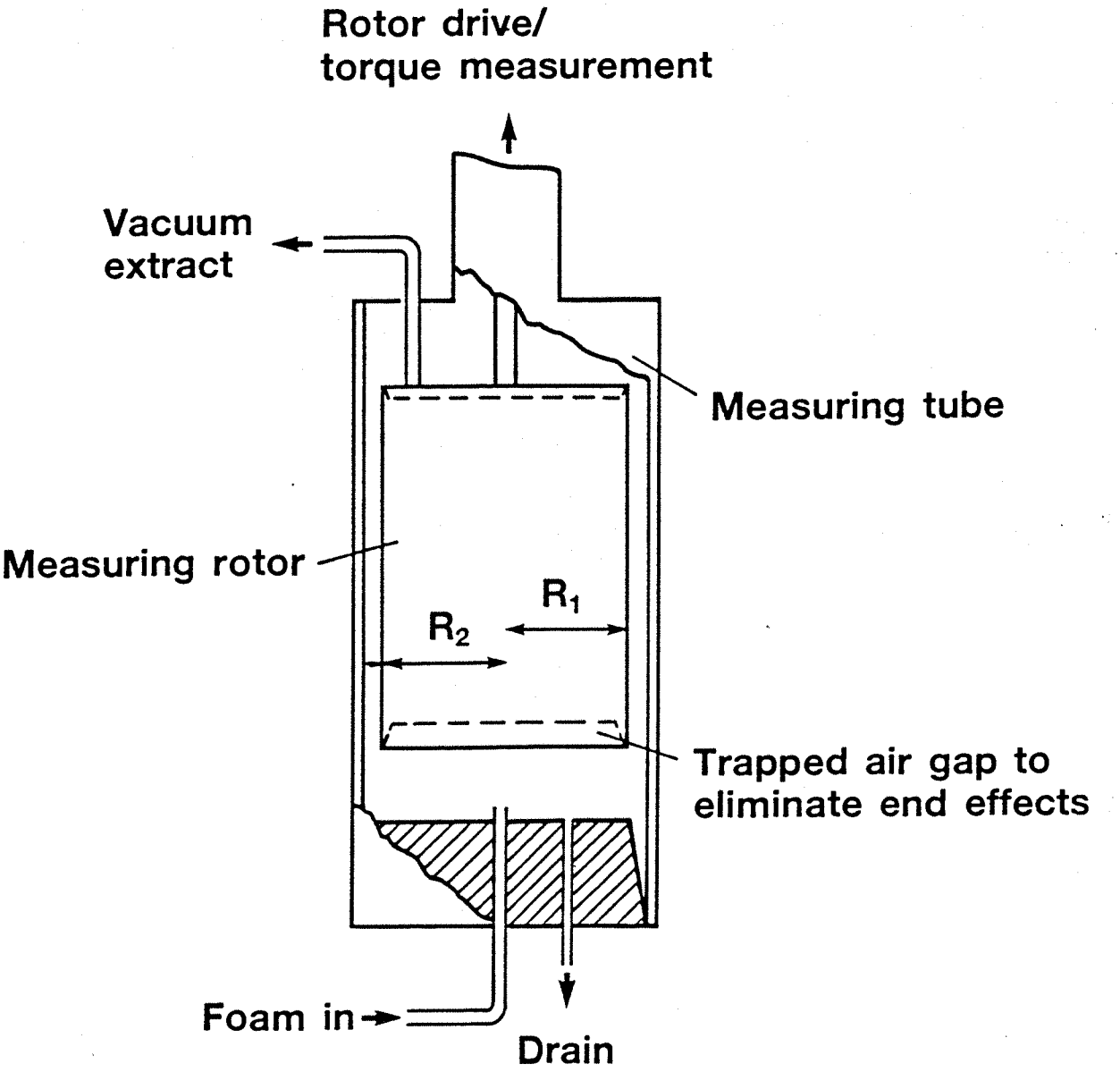

Figure 4c Exploded view of measuring system.

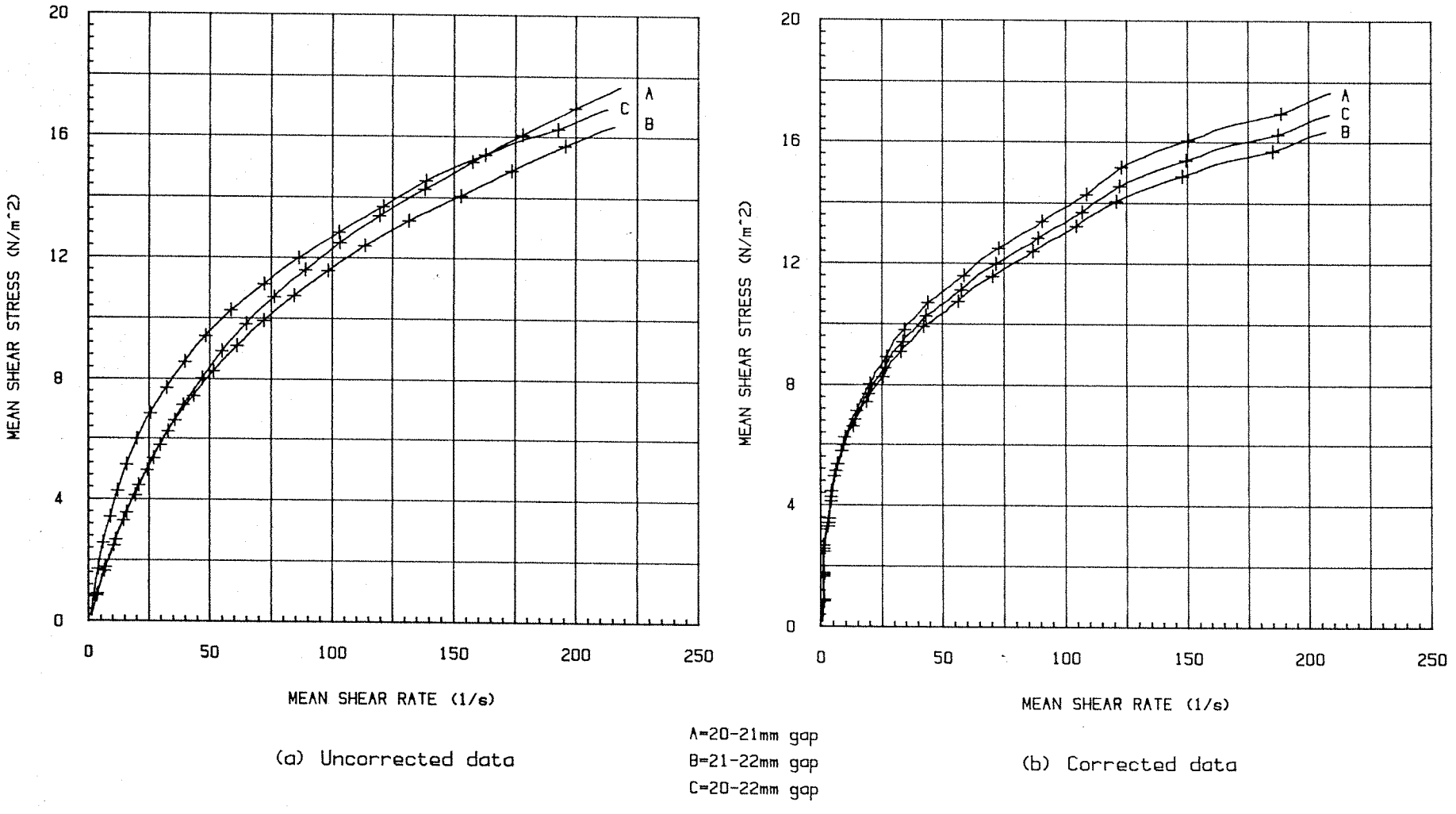

FIGURE 5. 70% QUALITY FOAM: FLOW CURVES AS MEASURED AND CORRECTED FOR WALL SLIP

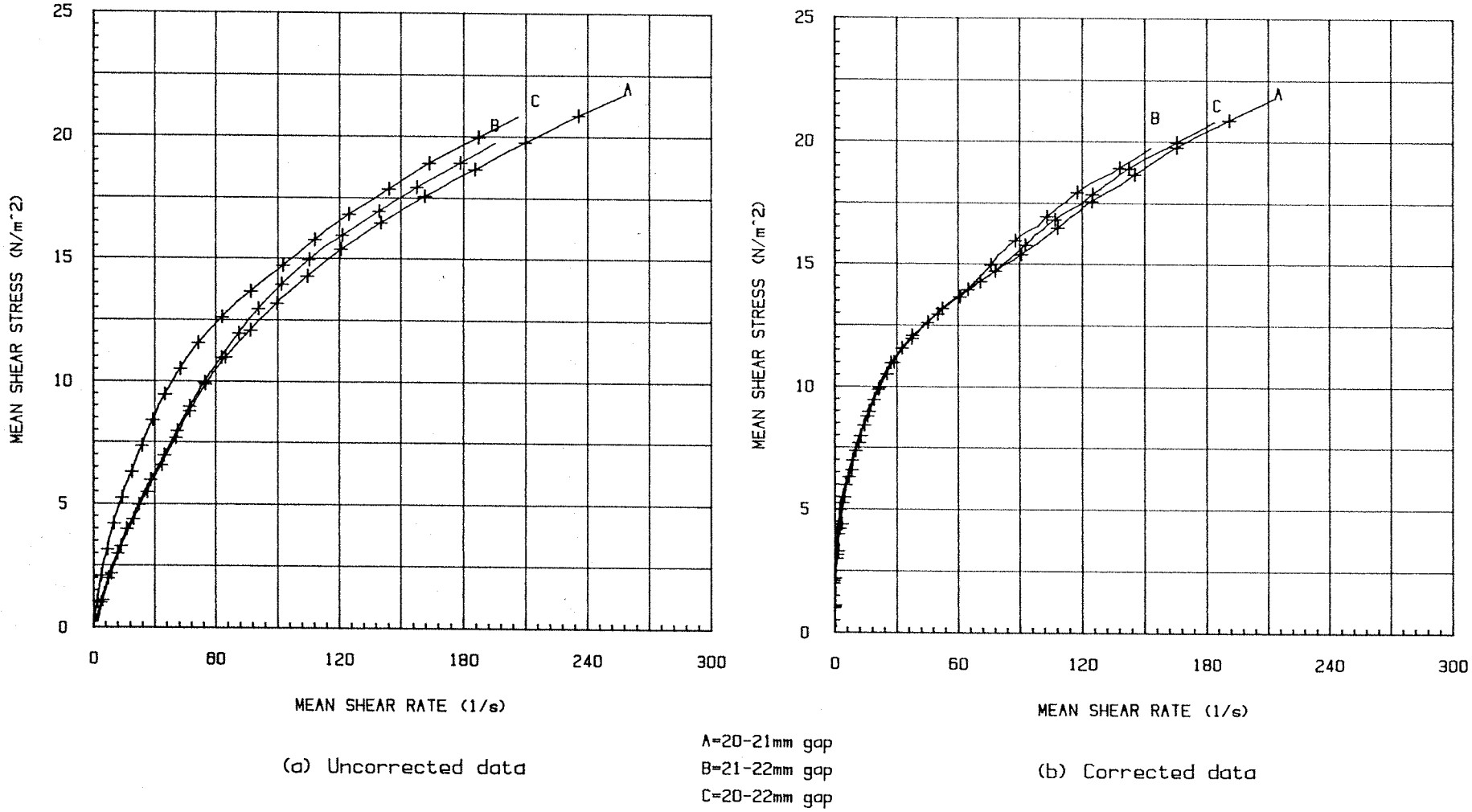

FIGURE 6. 75% QUALITY FOAM: FLOW CURVES AS MEASURED AND CORRECTED FOR WALL SLIP

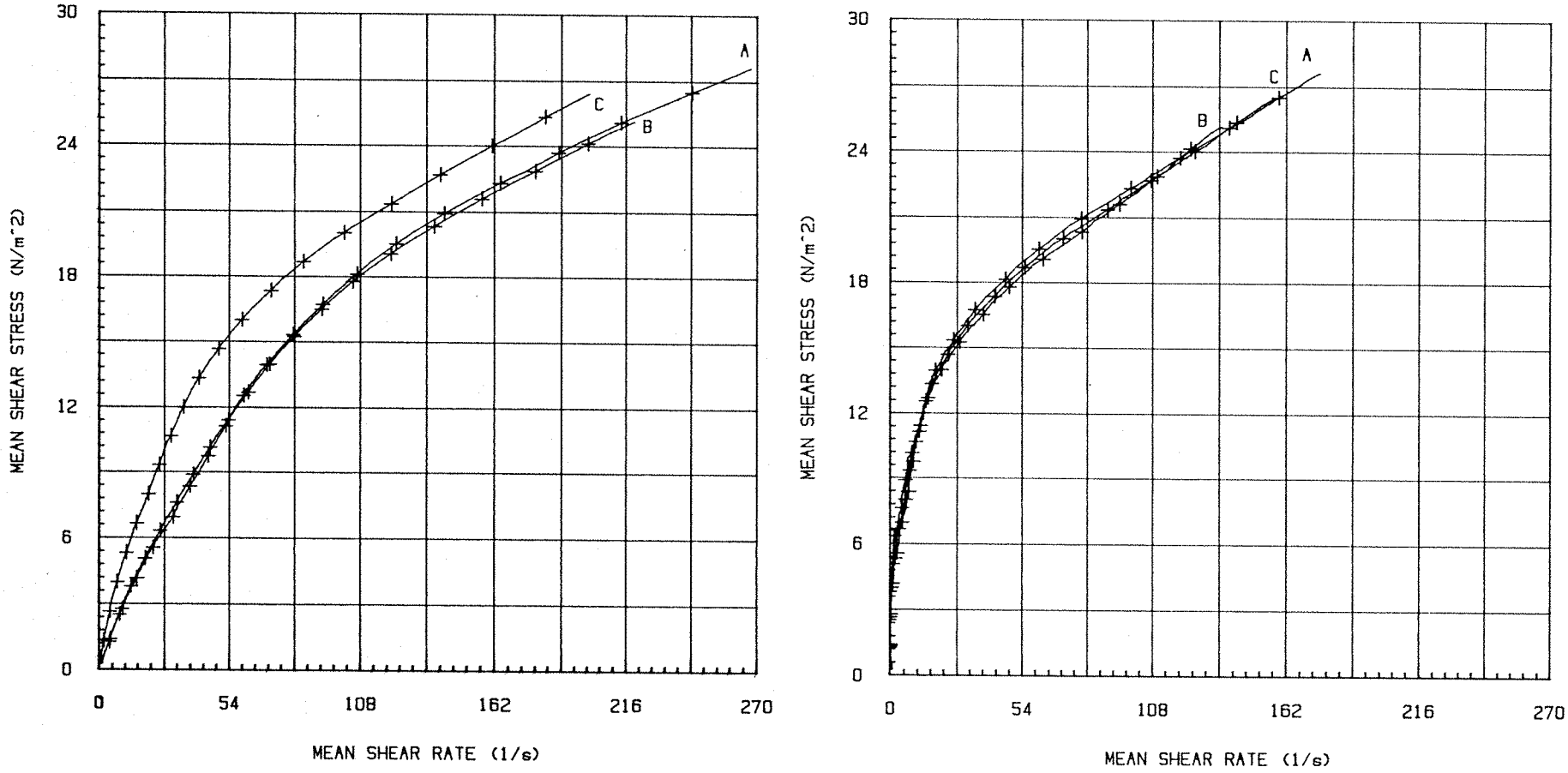

(a) Uncorrected data

A=20-21mm gap
B=21-22mm gap
C=20-22mm gap

(b) Corrected data

FIGURE 7. 80% QUALITY FOAM: FLOW CURVES AS MEASURED AND CORRECTED FOR WALL SLIP

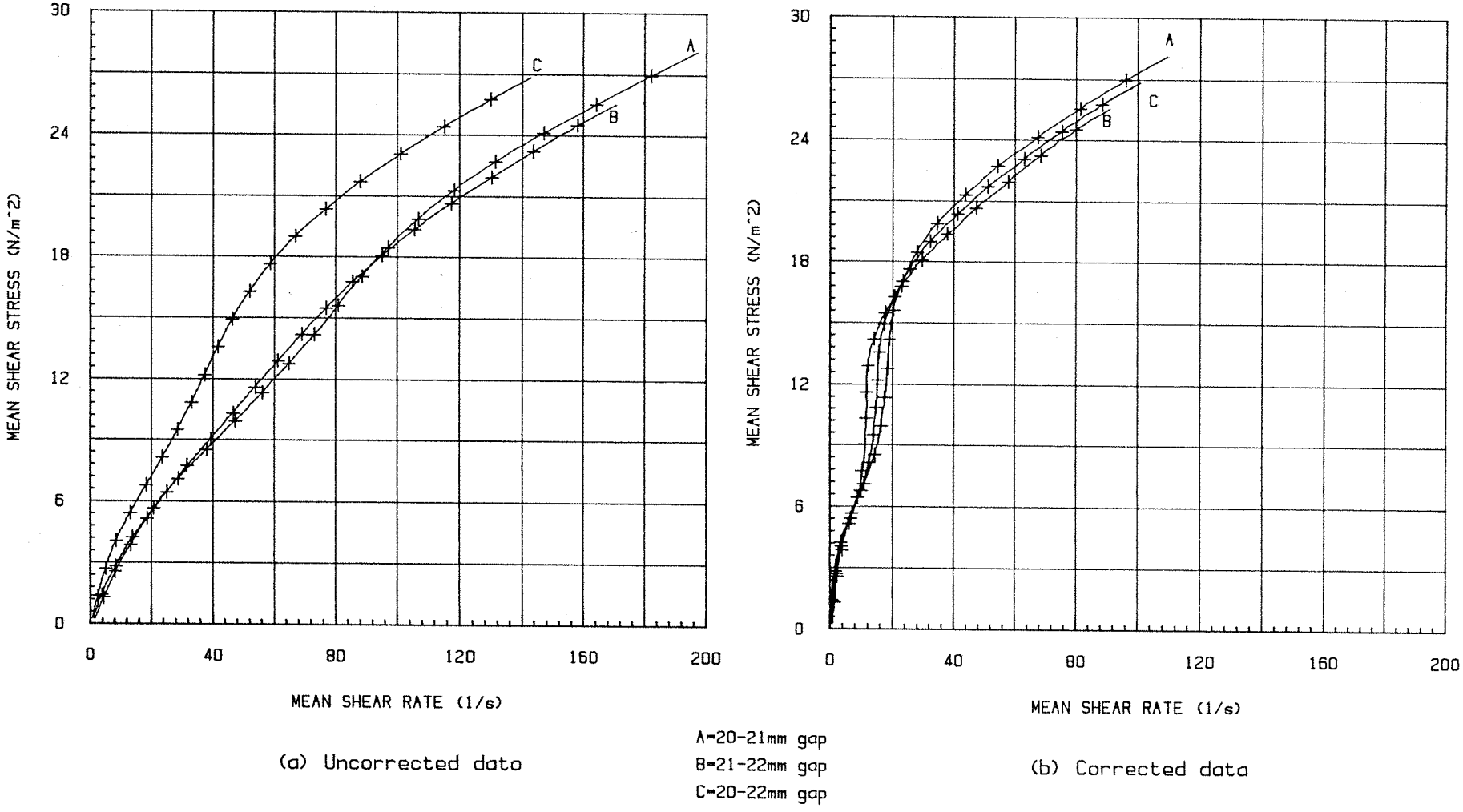

(a) Uncorrected data

A=20-21mm gap
B=21-22mm gap
C=20-22mm gap

(b) Corrected data

FIGURE 8. 85% QUALITY FOAM: FLOW CURVES AS MEASURED AND CORRECTED FOR WALL SLIP

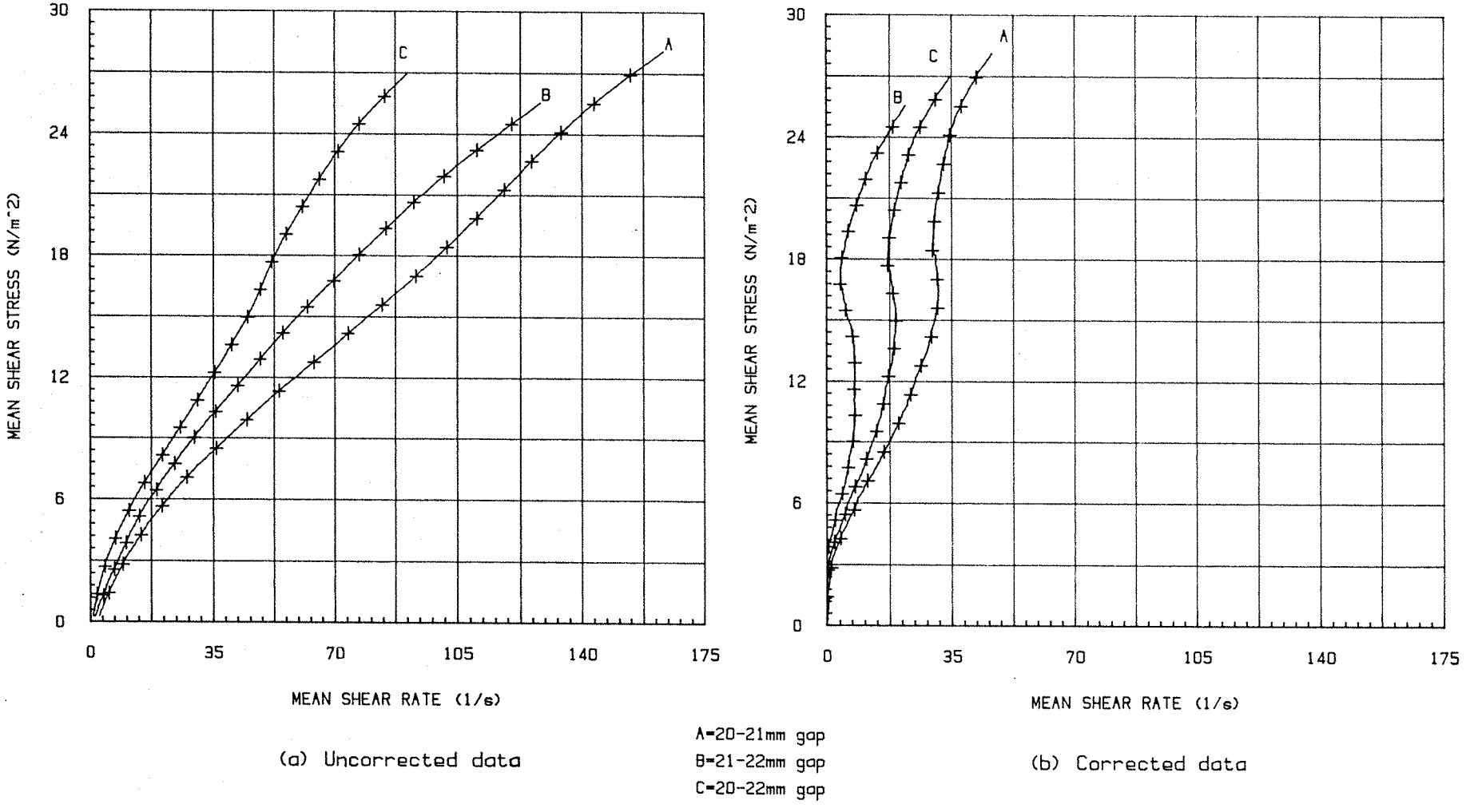

FIGURE 9. 90% QUALITY FOAM: FLOW CURVES AS MEASURED AND CORRECTED FOR WALL SLIP

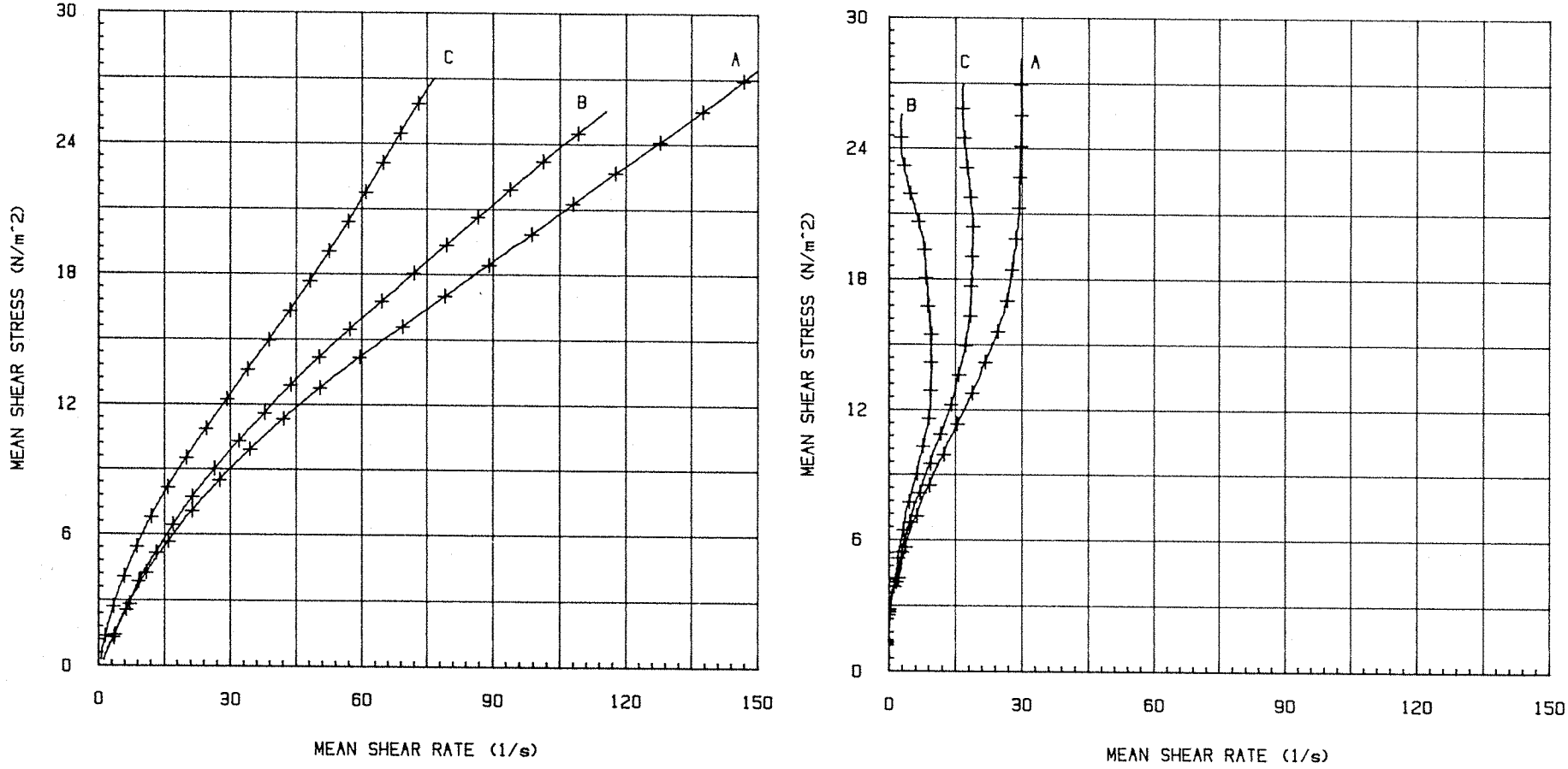

FIGURE 10. 95% QUALITY FOAM: FLOW CURVES AS MEASURED AND CORRECTED FOR WALL SLIP

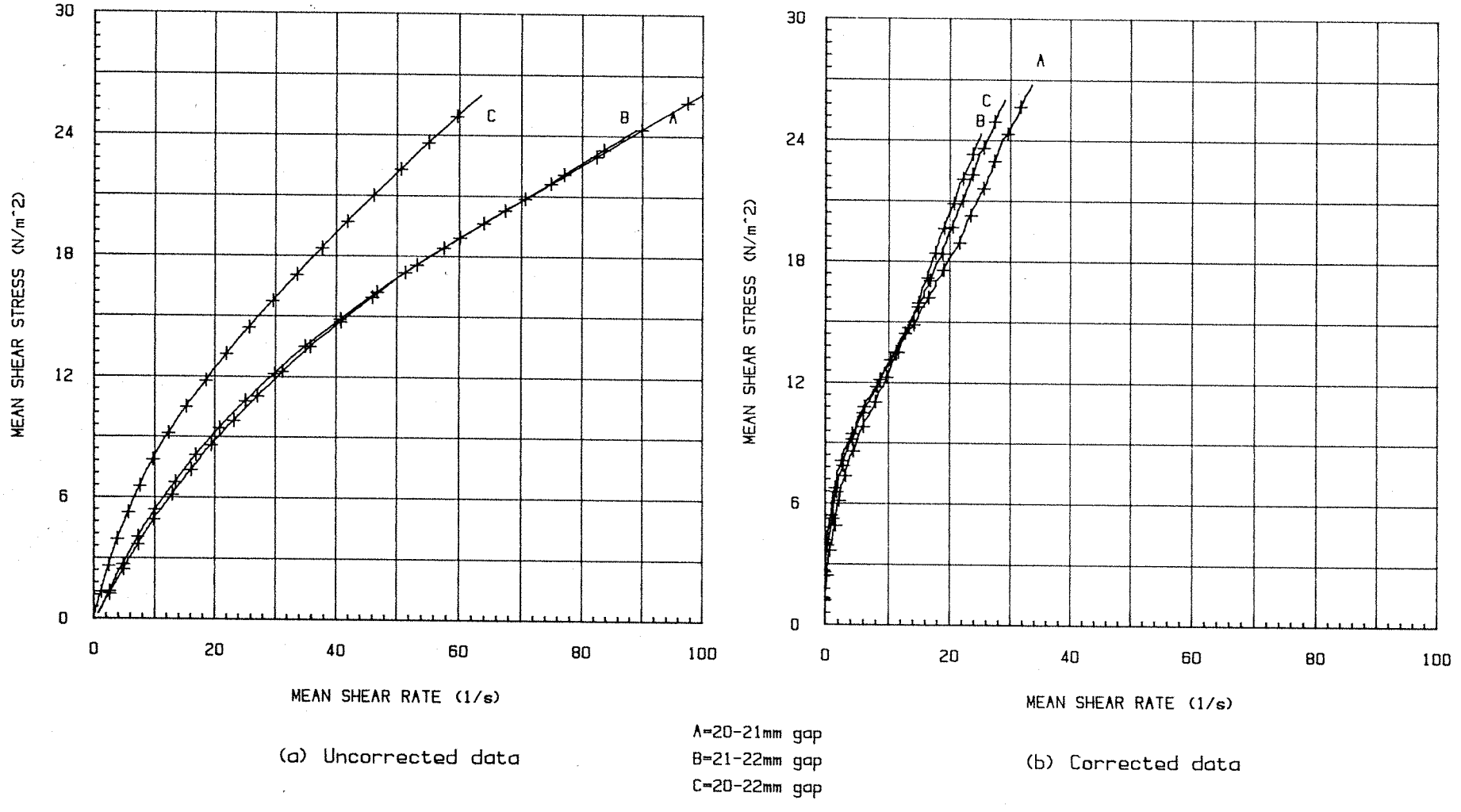

FIGURE 11. 98% QUALITY FOAM: FLOW CURVES AS MEASURED AND CORRECTED FOR WALL SLIP

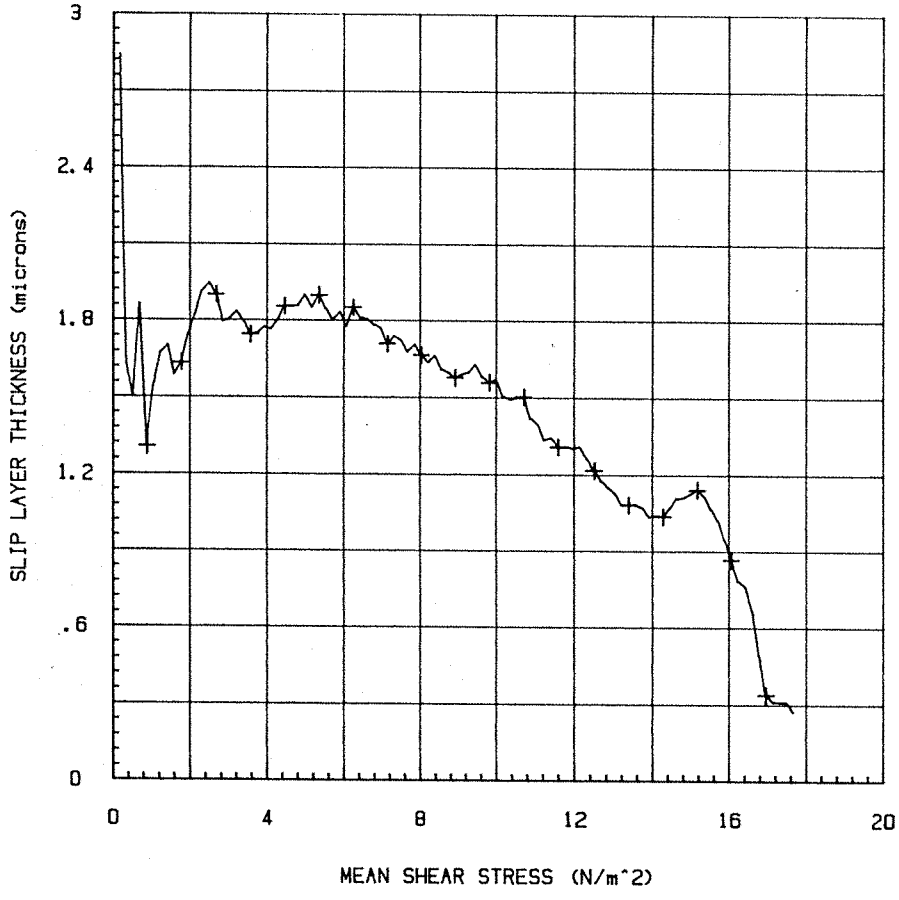

(a) Slip layer width variation

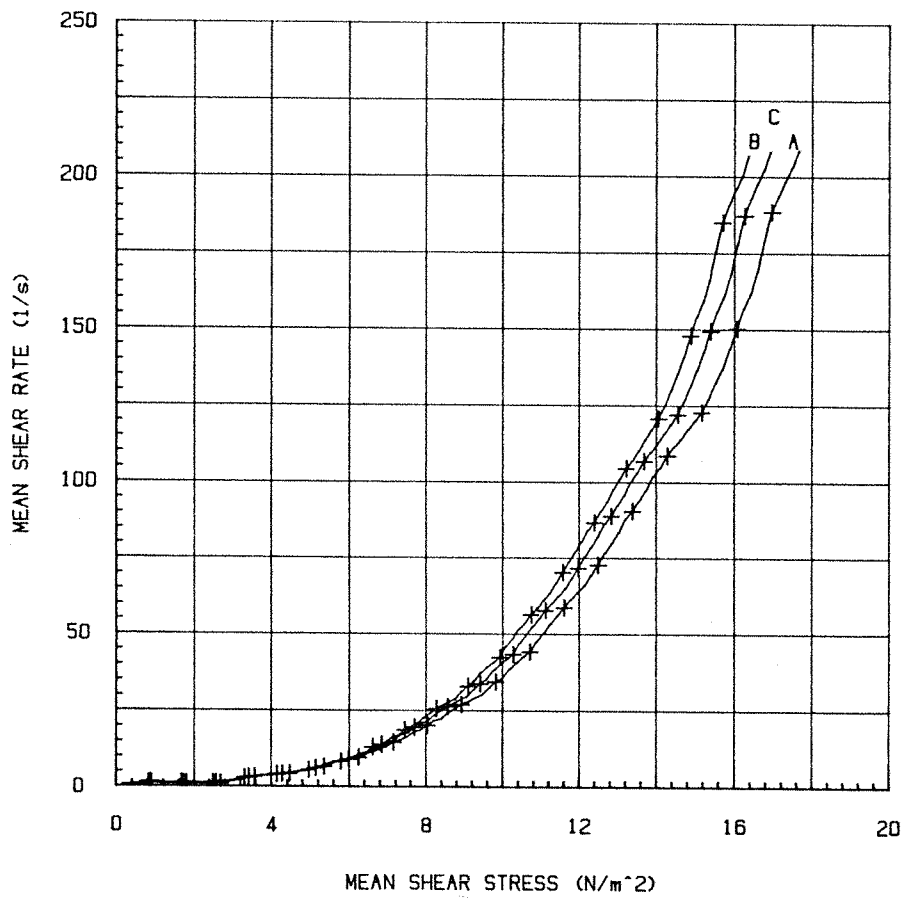

(b) Corrected foam flow curves

A=20-21mm gap
B=21-22mm gap
C=20-22mm gap

FIGURE 12. 70% QUALITY FOAM: SLIP LAYER WIDTH AND FOAM SHEAR RATE (v) SHEAR STRESS

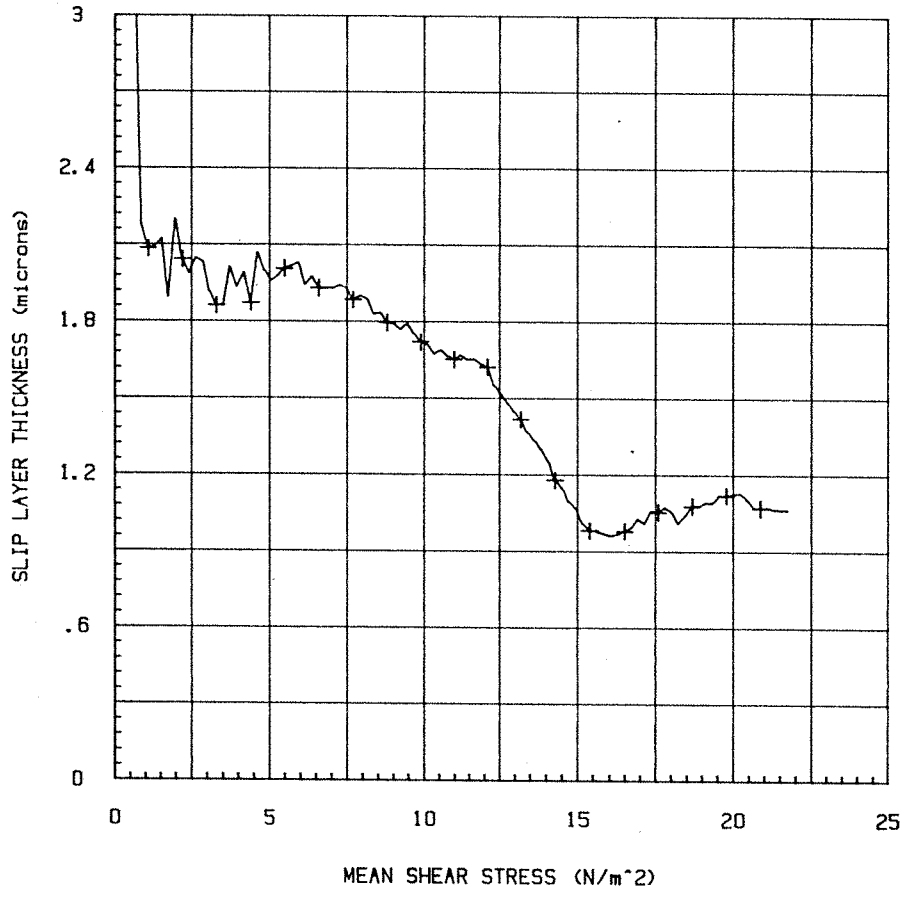

(a) Slip layer width variation

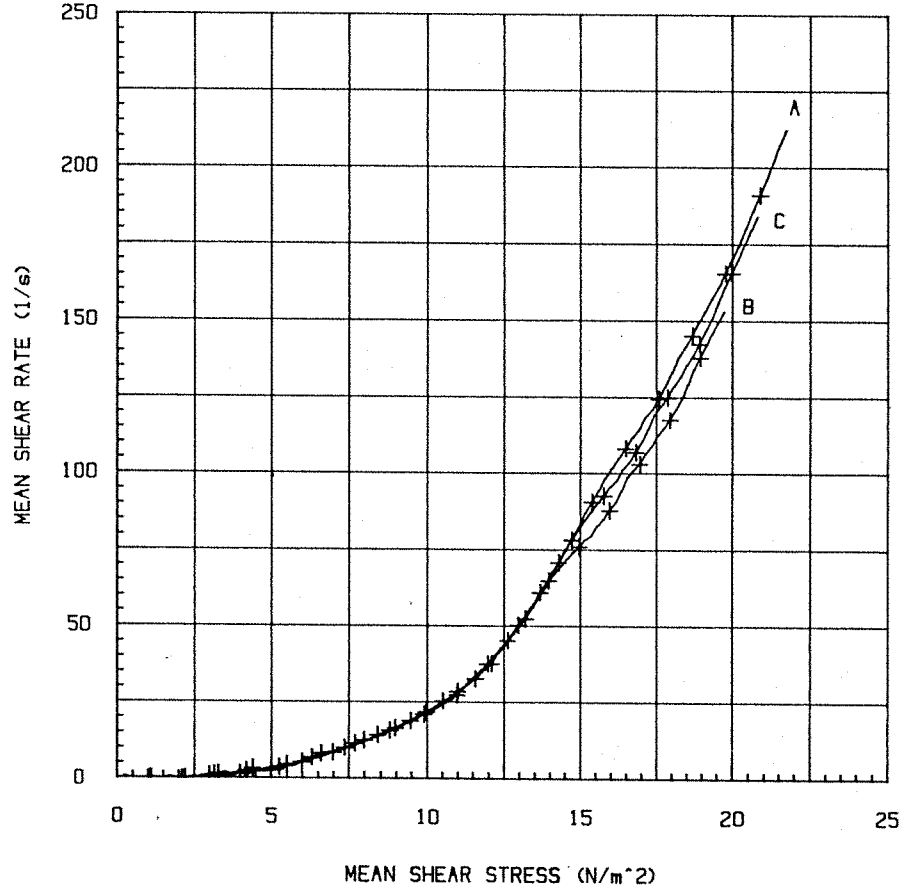

A=20-21mm gap
B=21-22mm gap
C=20-22mm gap

(b) Corrected foam flow curves

FIGURE 13. 75% QUALITY FOAM: SLIP LAYER WIDTH AND FOAM SHEAR RATE (v) SHEAR STRESS

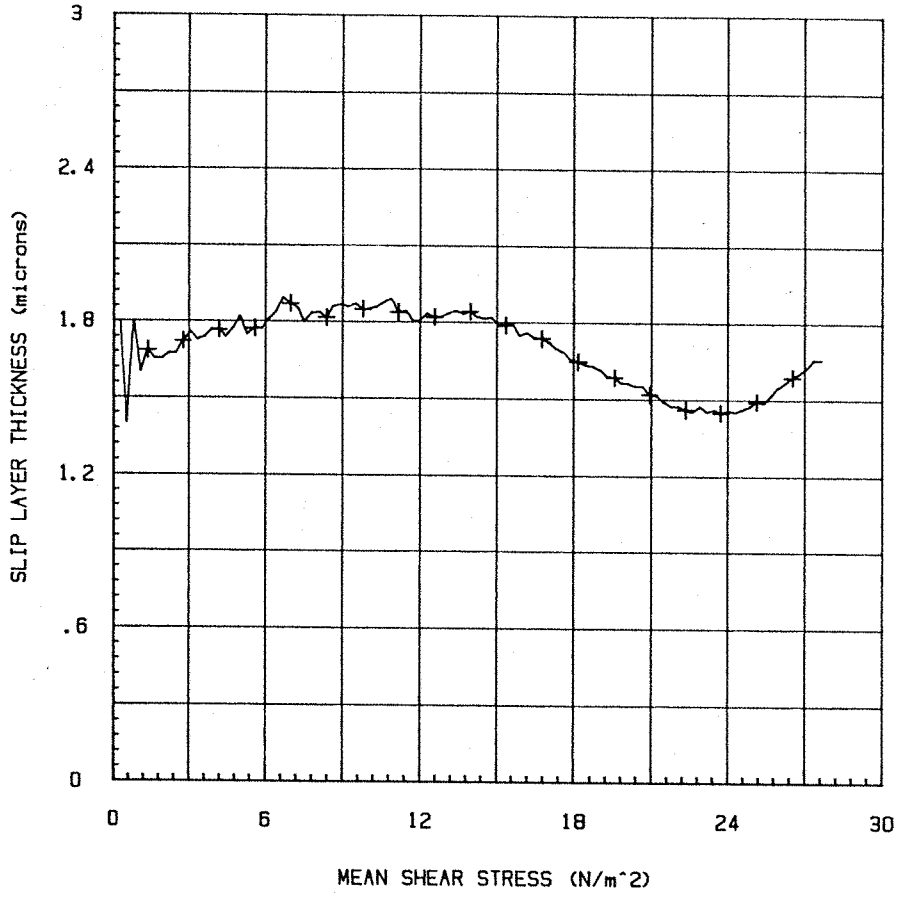

(a) Slip layer width variation

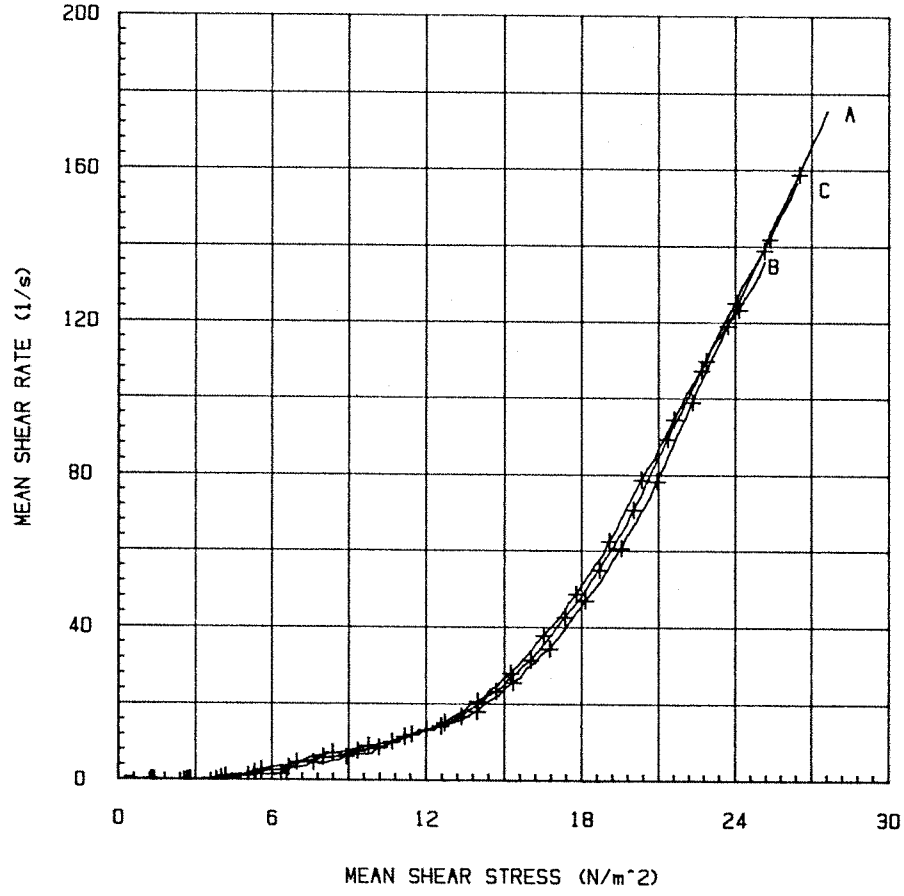

A=20-21mm gap
B=21-22mm gap
C=20-22mm gap

(b) Corrected foam flow curves

FIGURE 14. 80% QUALITY FOAM: SLIP LAYER WIDTH AND FOAM SHEAR RATE (v) SHEAR STRESS

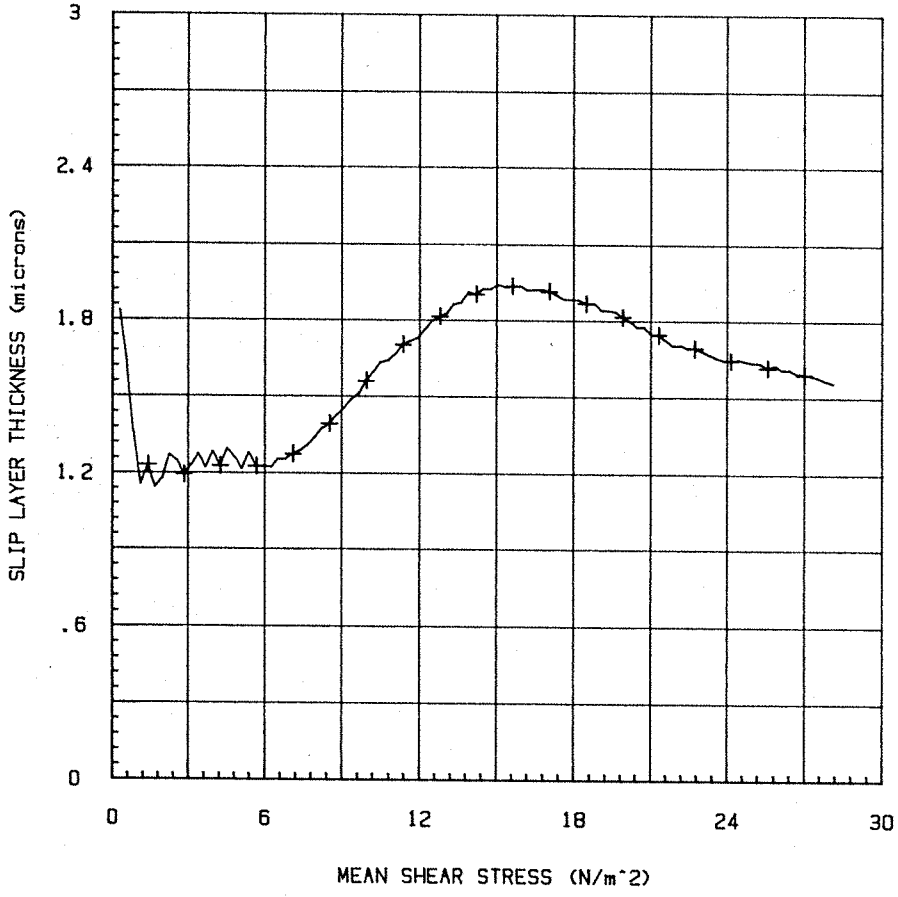

(a) Slip layer width variation

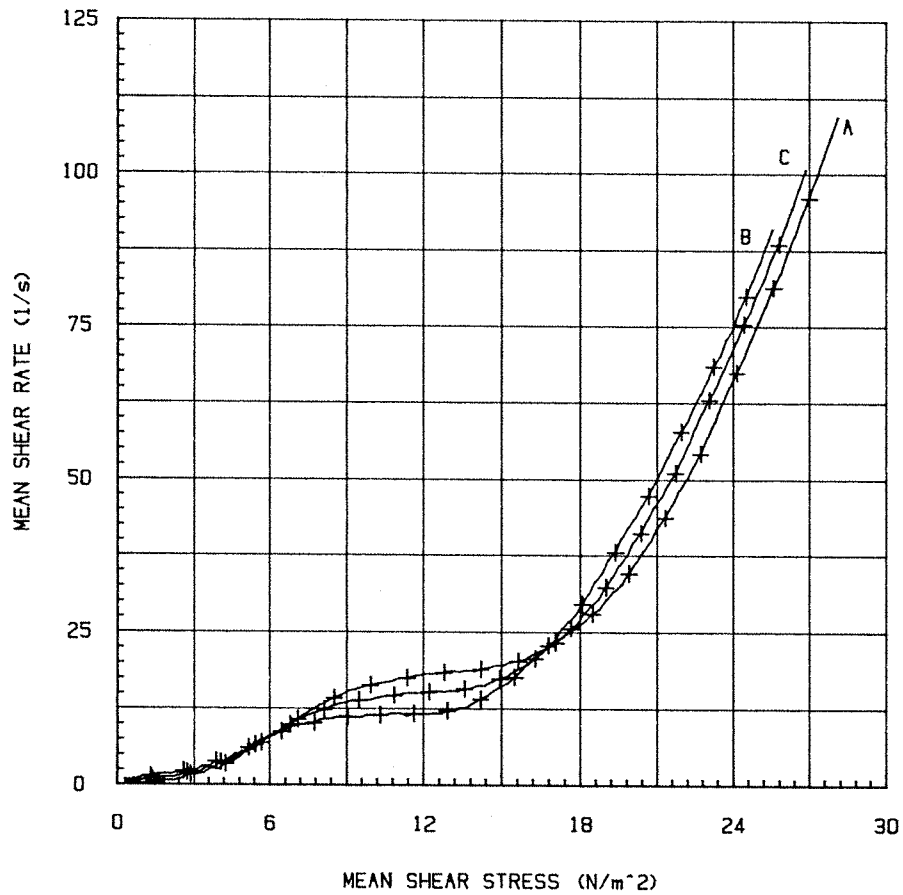

A=20-21mm gap
B=21-22mm gap
C=20-22mm gap

(b) Corrected foam flow curves

FIGURE 15. 85% QUALITY FOAM: SLIP LAYER WIDTH AND FOAM SHEAR RATE (v) SHEAR STRESS

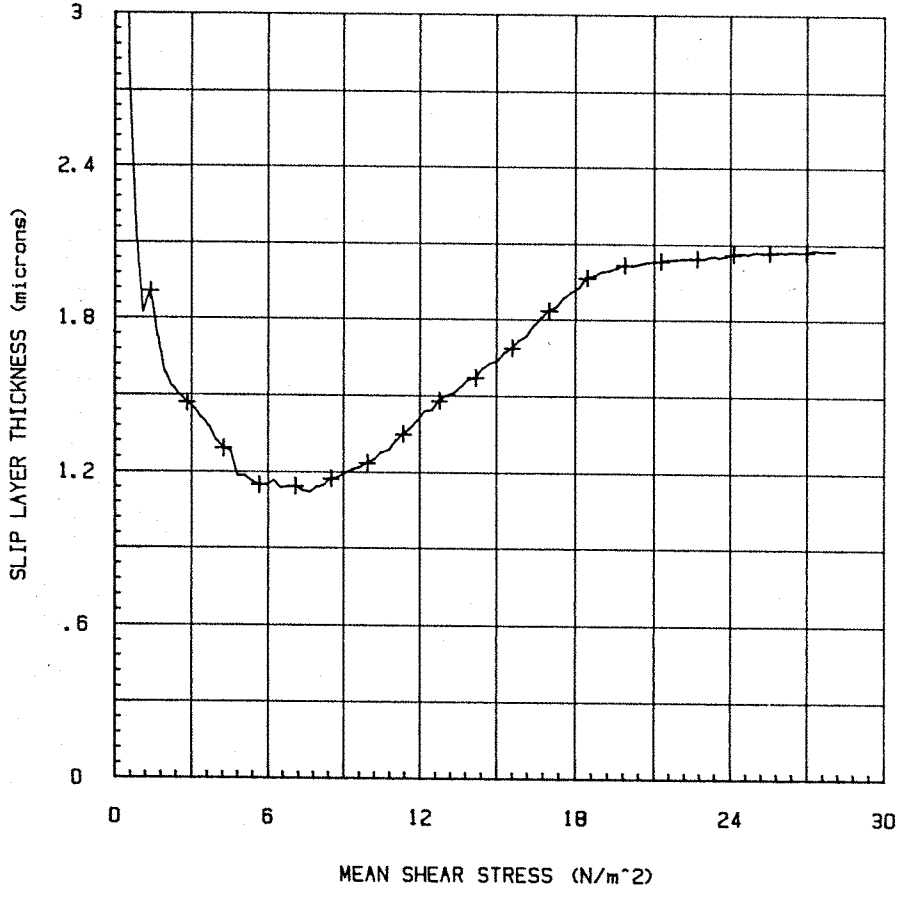

(a) Slip layer width variation

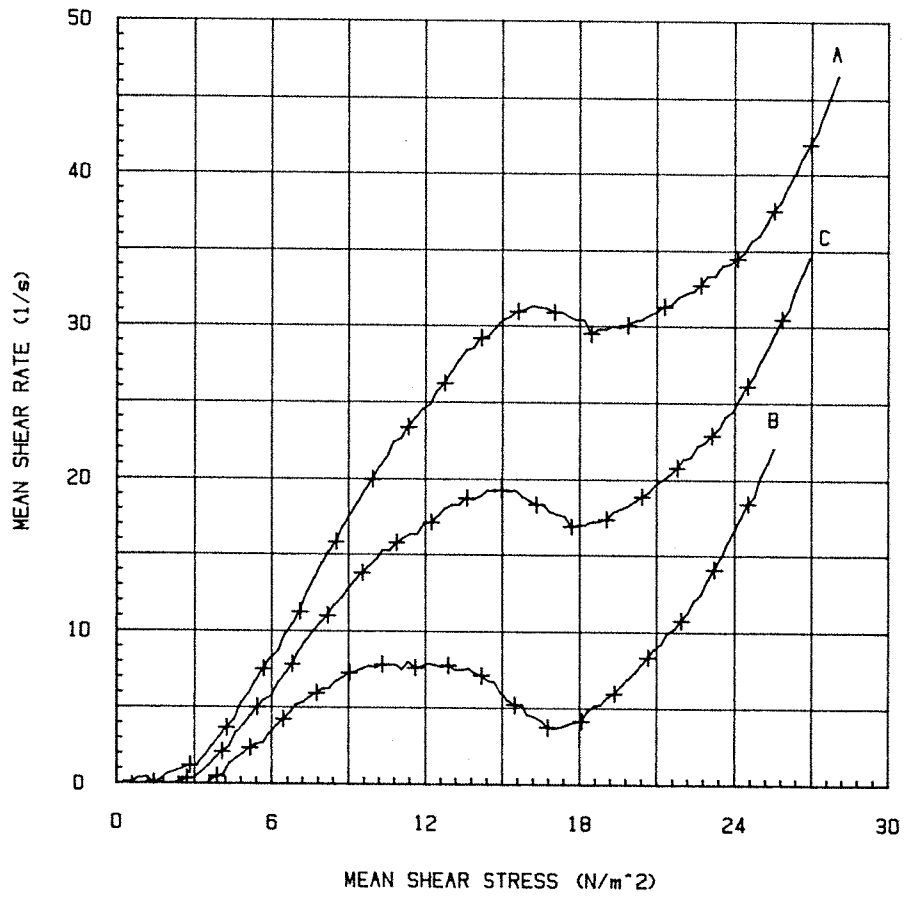

A=20-21mm gap
B=21-22mm gap
C=20-22mm gap

(b) Corrected foam flow curves

FIGURE 16. 90% QUALITY FOAM: SLIP LAYER WIDTH AND FOAM SHEAR RATE (v) SHEAR STRESS

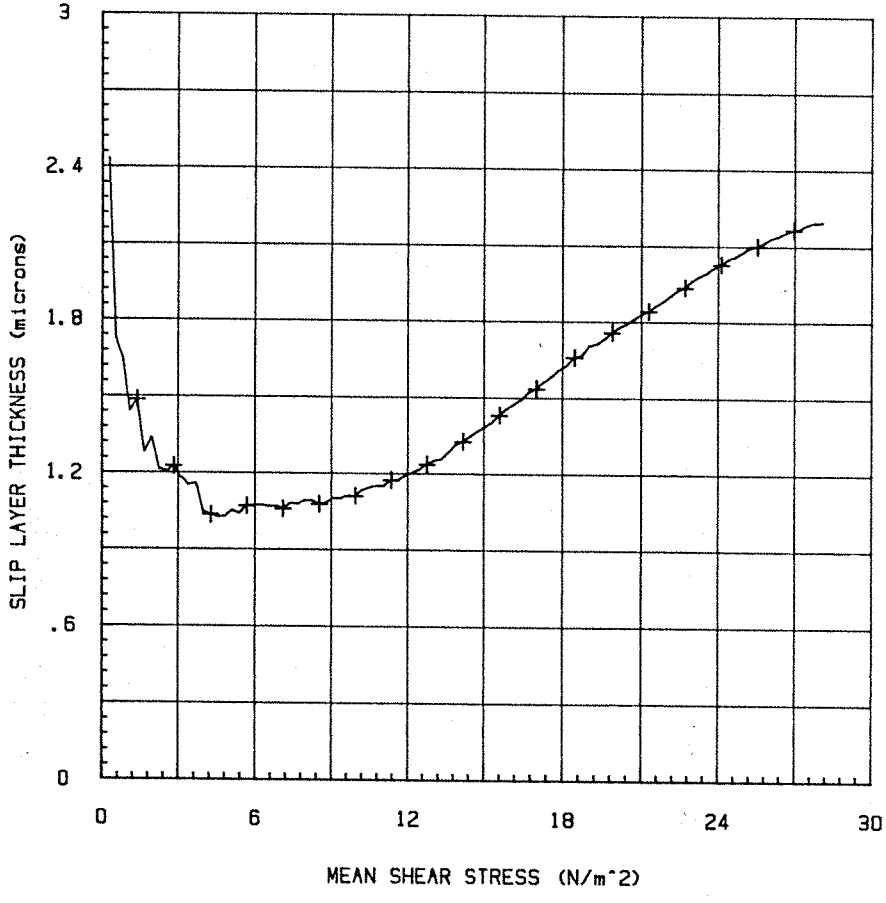

(a) Slip layer width variation

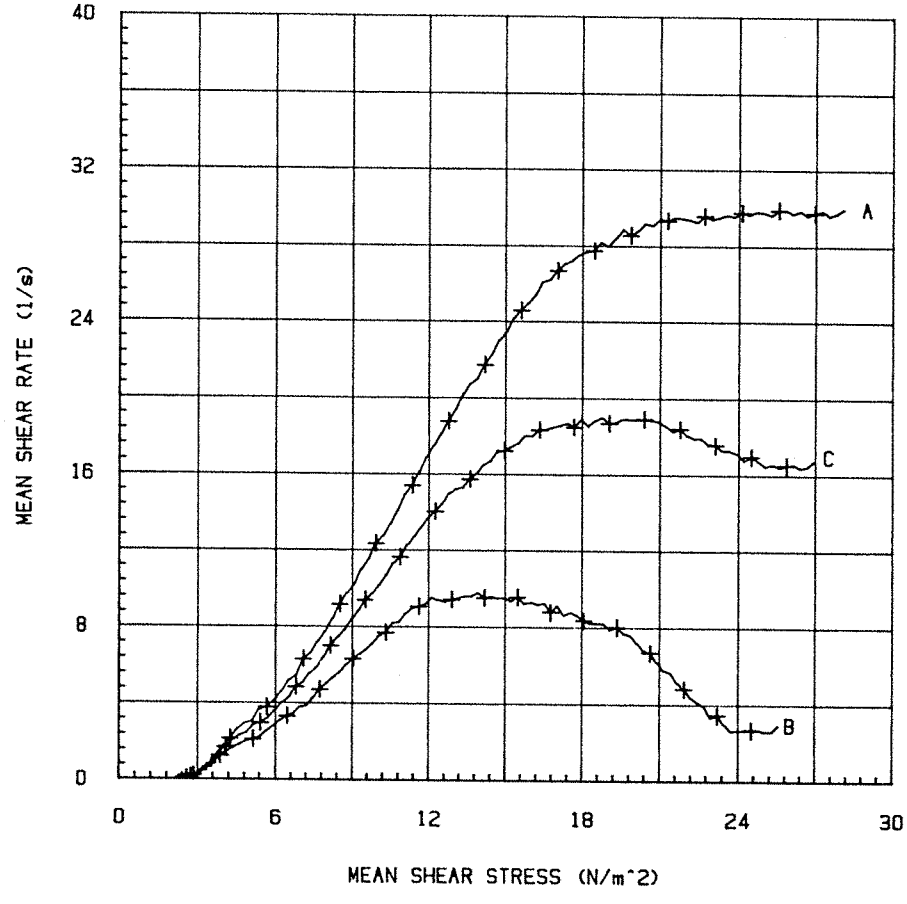

A=20-21mm gap
B=21-22mm gap
C=20-22mm gap

(b) Corrected foam flow curves

FIGURE 17. 95% QUALITY FOAM: SLIP LAYER WIDTH AND FOAM SHEAR RATE (v) SHEAR STRESS

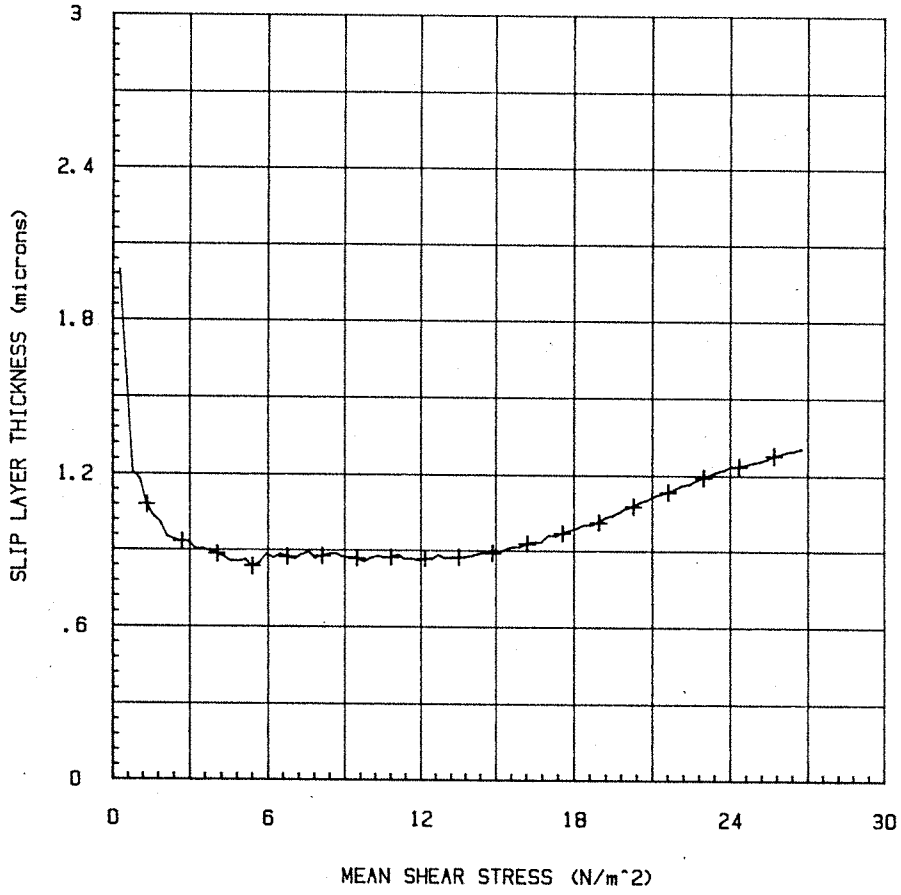

(a) Slip layer width variation

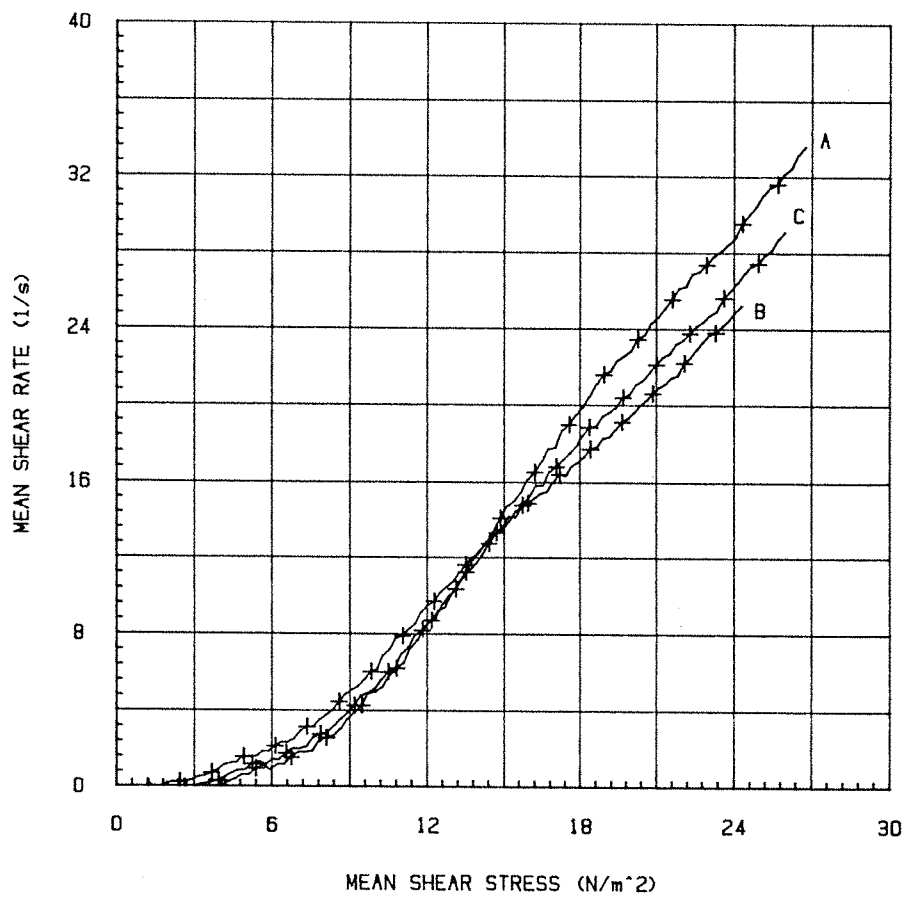

A=20-21mm gap
B=21-22mm gap
C=20-22mm gap

(b) Corrected foam flow curves

FIGURE 18. 98% QUALITY FOAM: SLIP LAYER WIDTH AND FOAM SHEAR RATE (v) SHEAR STRESS

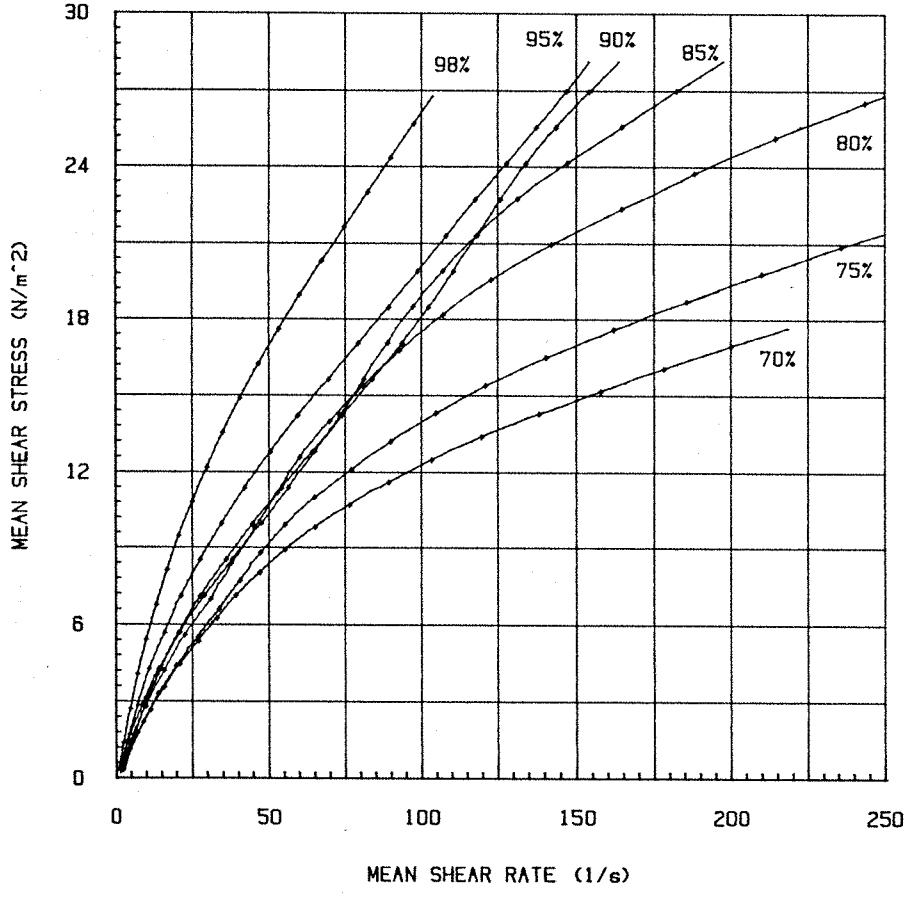

(a) Uncorrected data

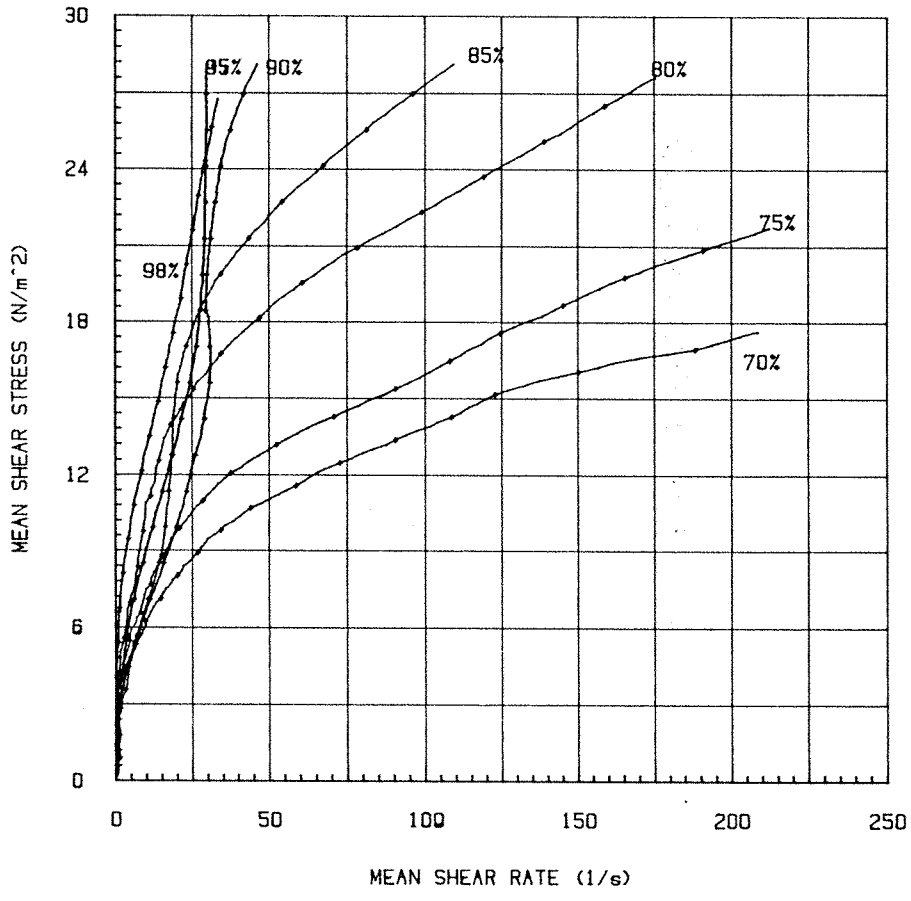

(b) Corrected data

FIGURE 19. CORRECTED AND UNCORRECTED FLOW CURVES FOR ALL FOAMS IN THE 20-21mm GAP

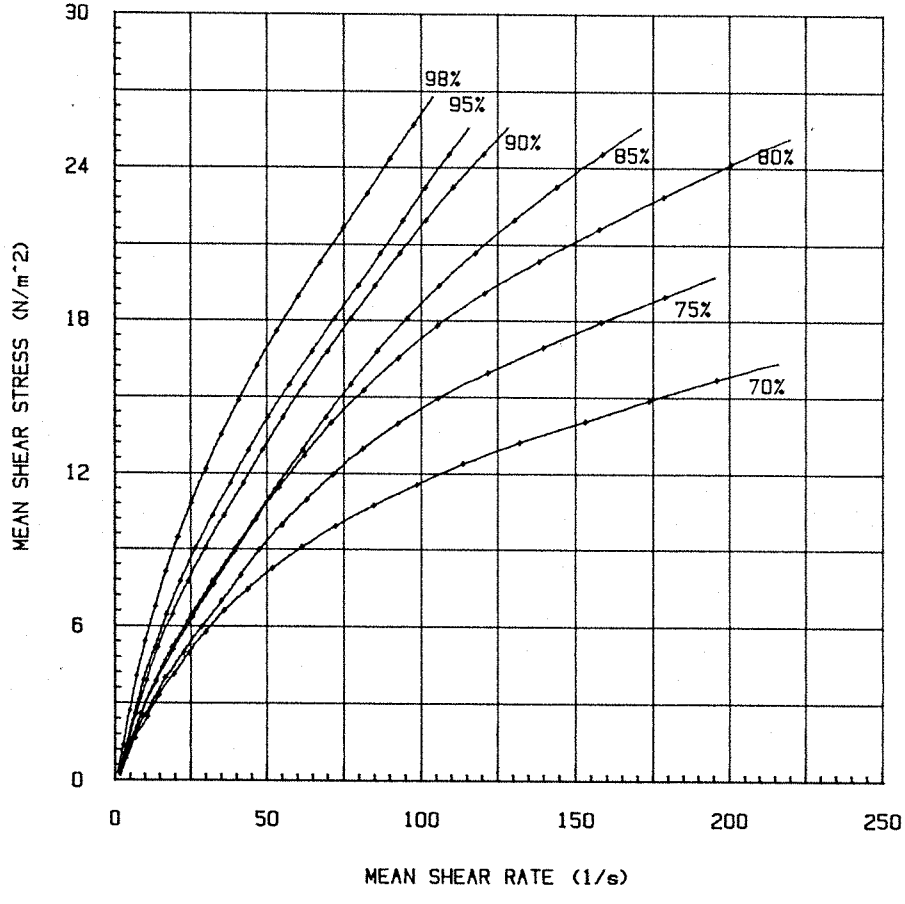

(a) Uncorrected data

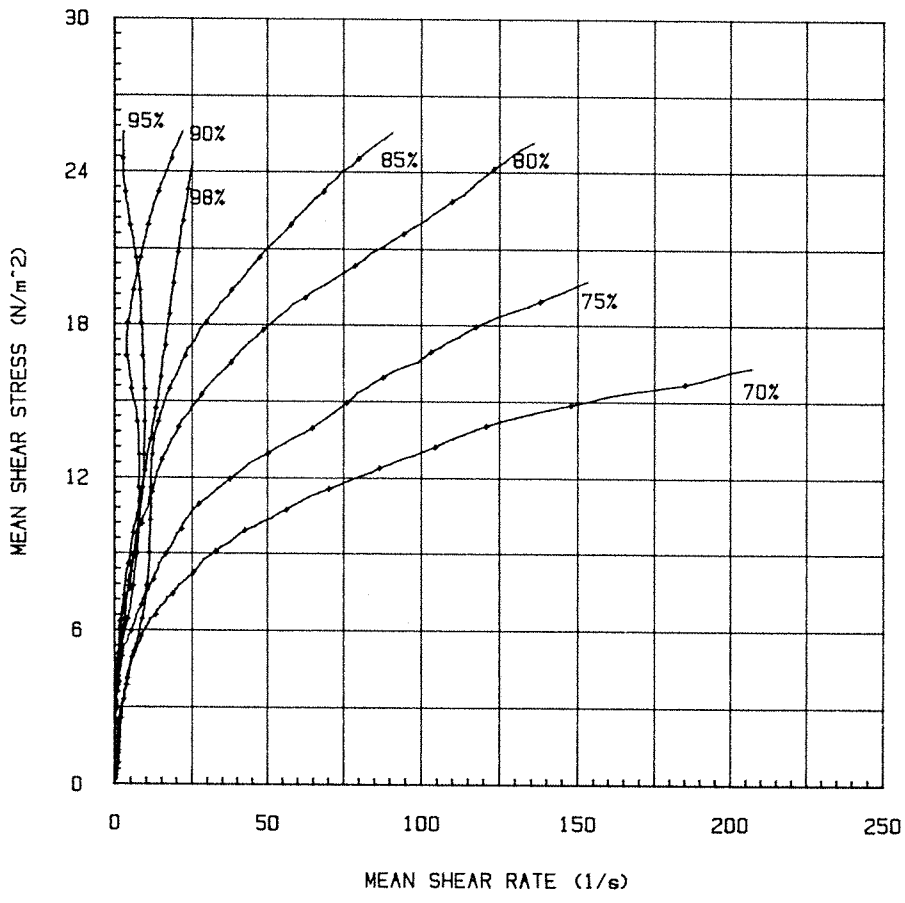

(b) Corrected data

FIGURE 20. CORRECTED AND UNCORRECTED FLOW CURVES FOR ALL FOAMS IN THE 21-22mm GAP

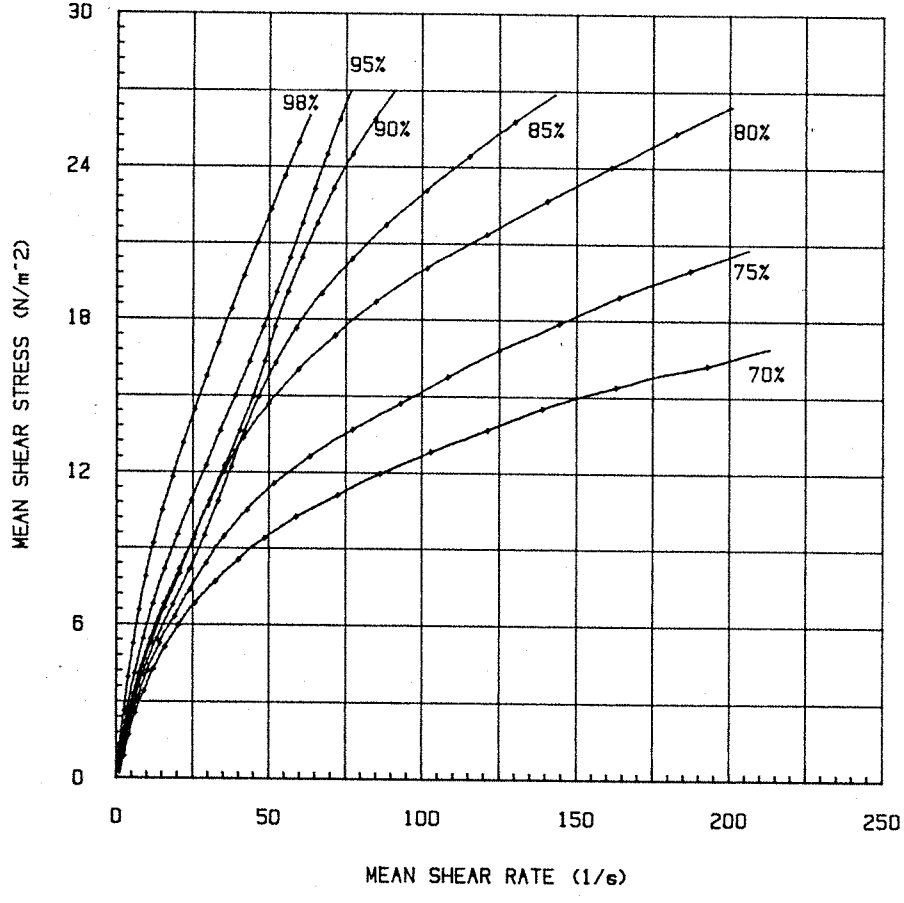

(a) Uncorrected data

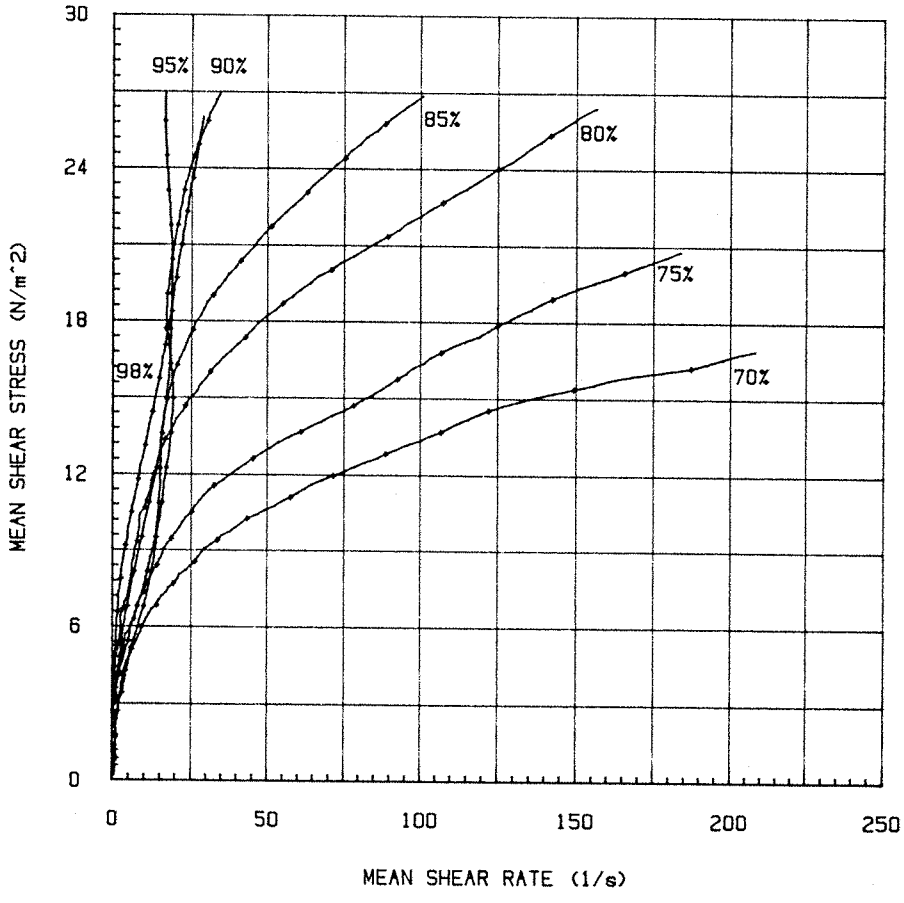

(b) Corrected data

FIGURE 21. CORRECTED AND UNCORRECTED FLOW CURVES FOR ALL FOAMS IN THE 20-22mm GAP

FIGURE 22. PHOTOGRAPH OF 70% QUALITY FOAM

SCALE 2.0mm

FIGURE 23. PHOTOGRAPH OF 75% QUALITY FOAM

SCALE 2.0mm

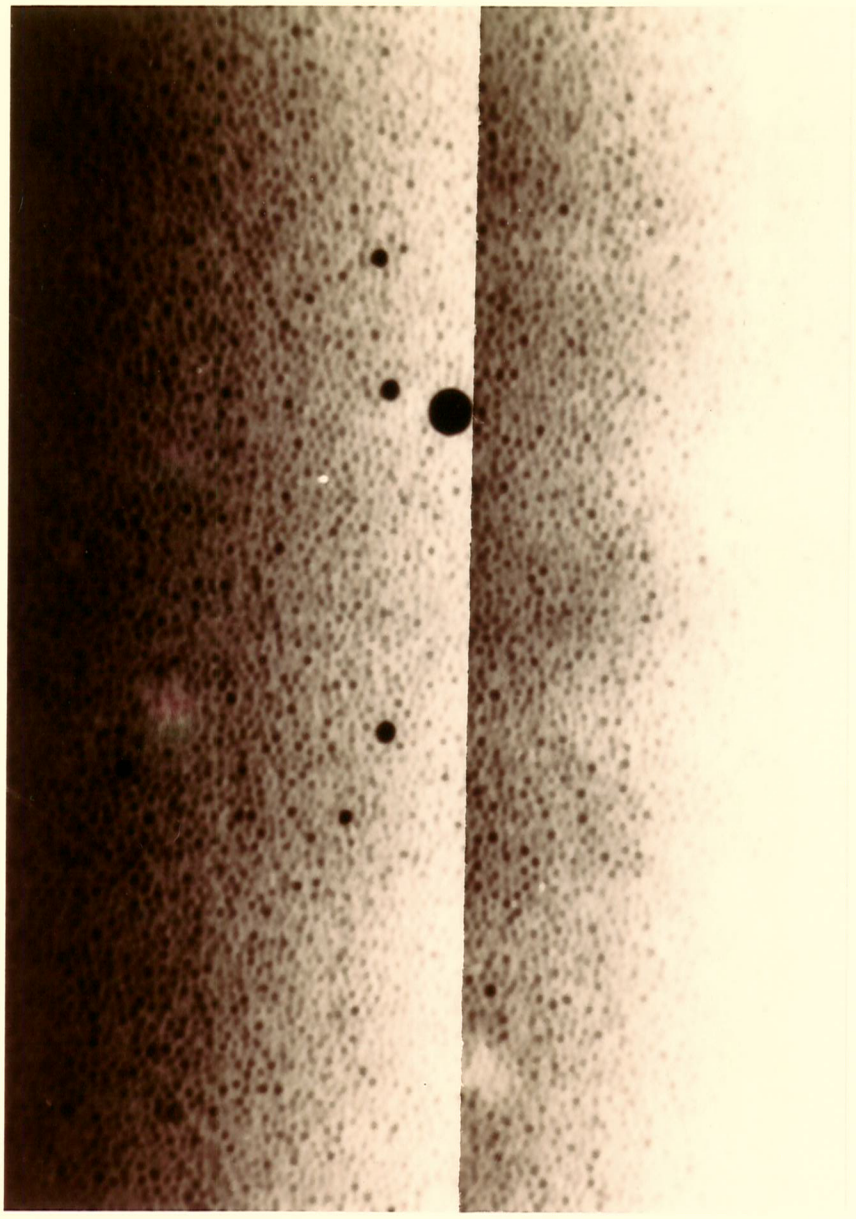

FIGURE 24. PHOTOGRAPH OF 80% QUALITY FOAM

SCALE 2.0mm

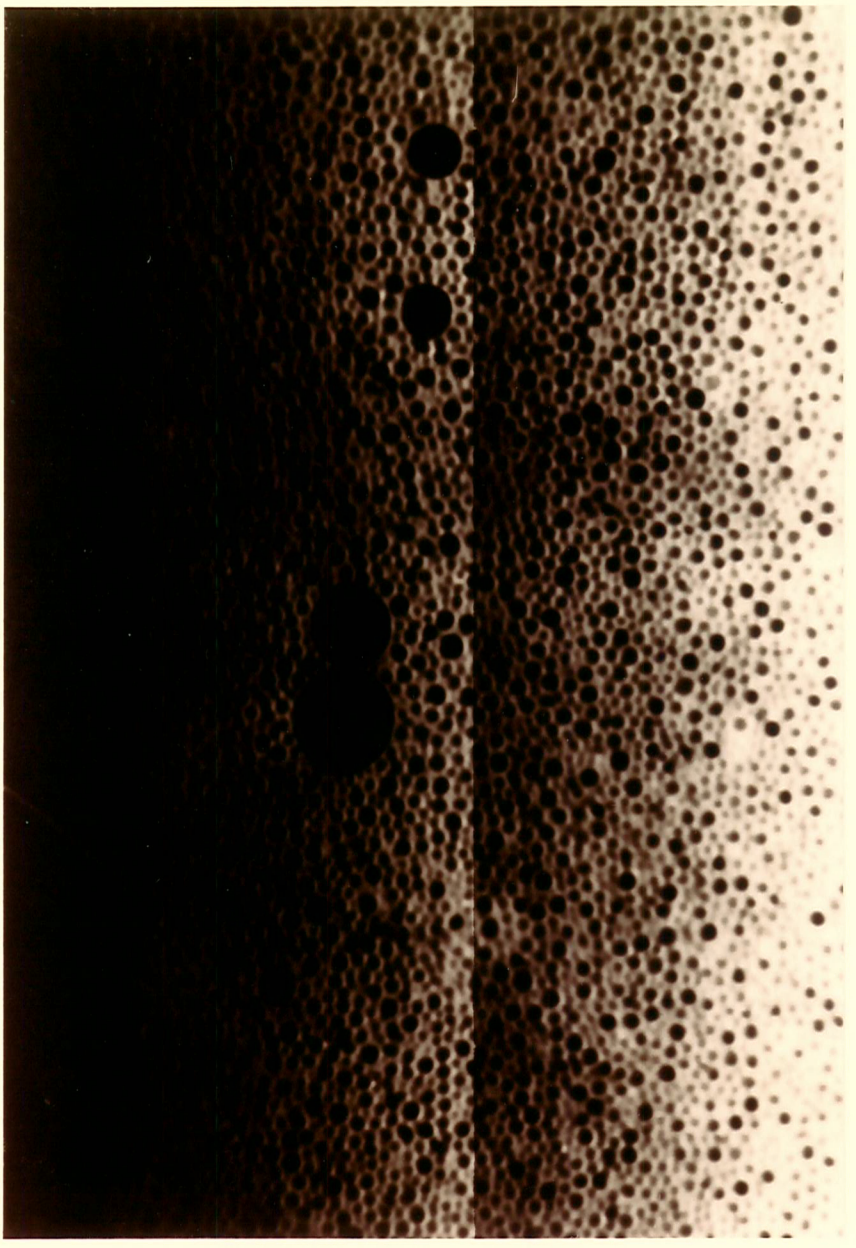

FIGURE 25. PHOTOGRAPH OF 85% QUALITY FOAM

SCALE 2.0mm

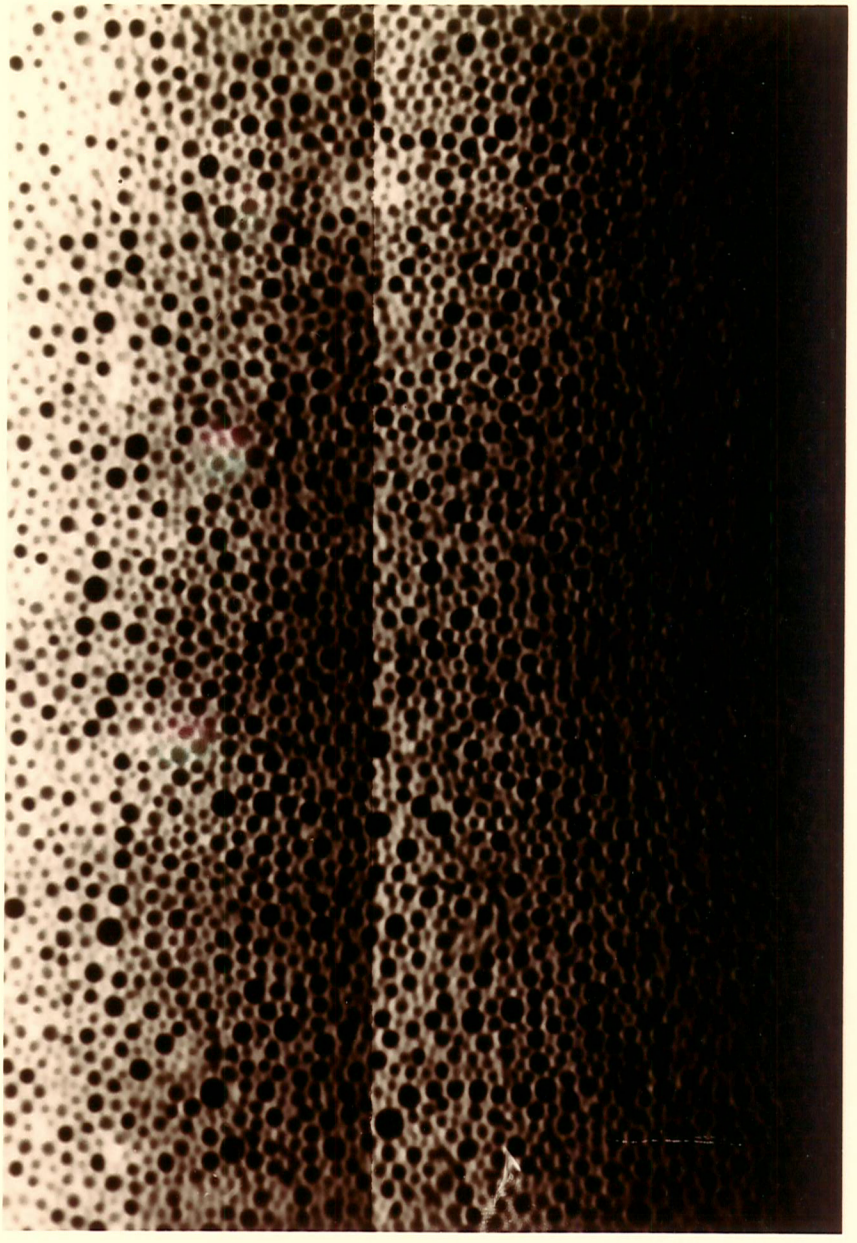

FIGURE 26. PHOTOGRAPH OF 90% QUALITY FOAM

SCALE 2.0mm

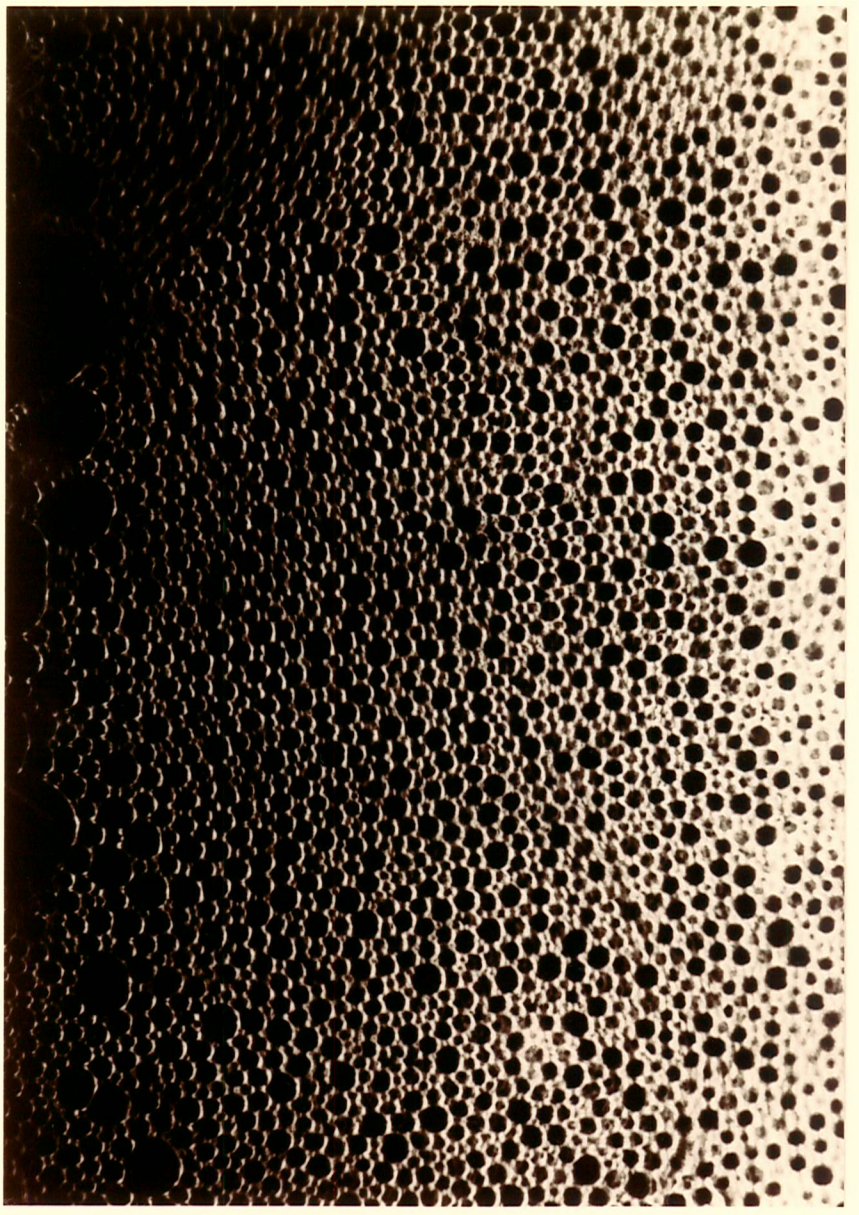

FIGURE 27. PHOTOGRAPH OF 95% QUALITY FOAM

SCALE 2.0mm

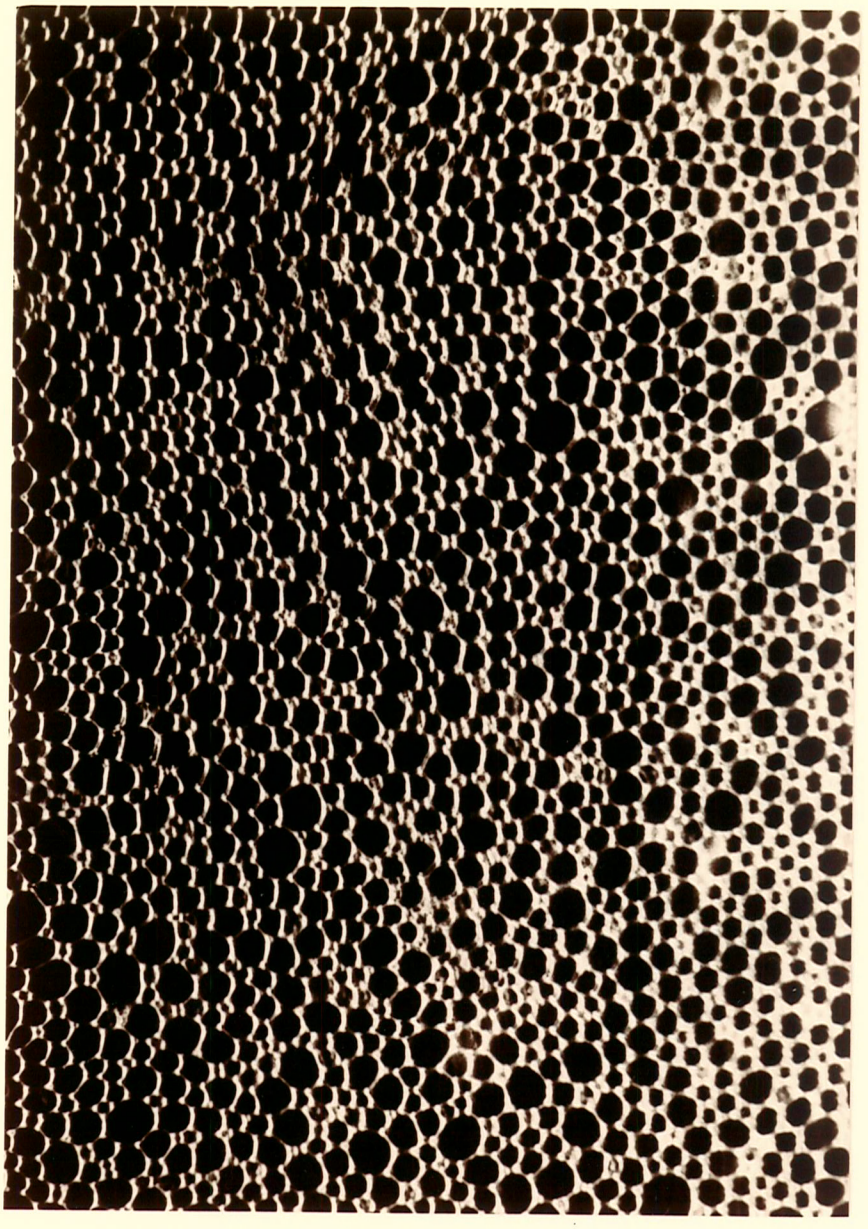

FIGURE 28. PHOTOGRAPH OF 98% QUALITY FOAM

SCALE 2.0mm

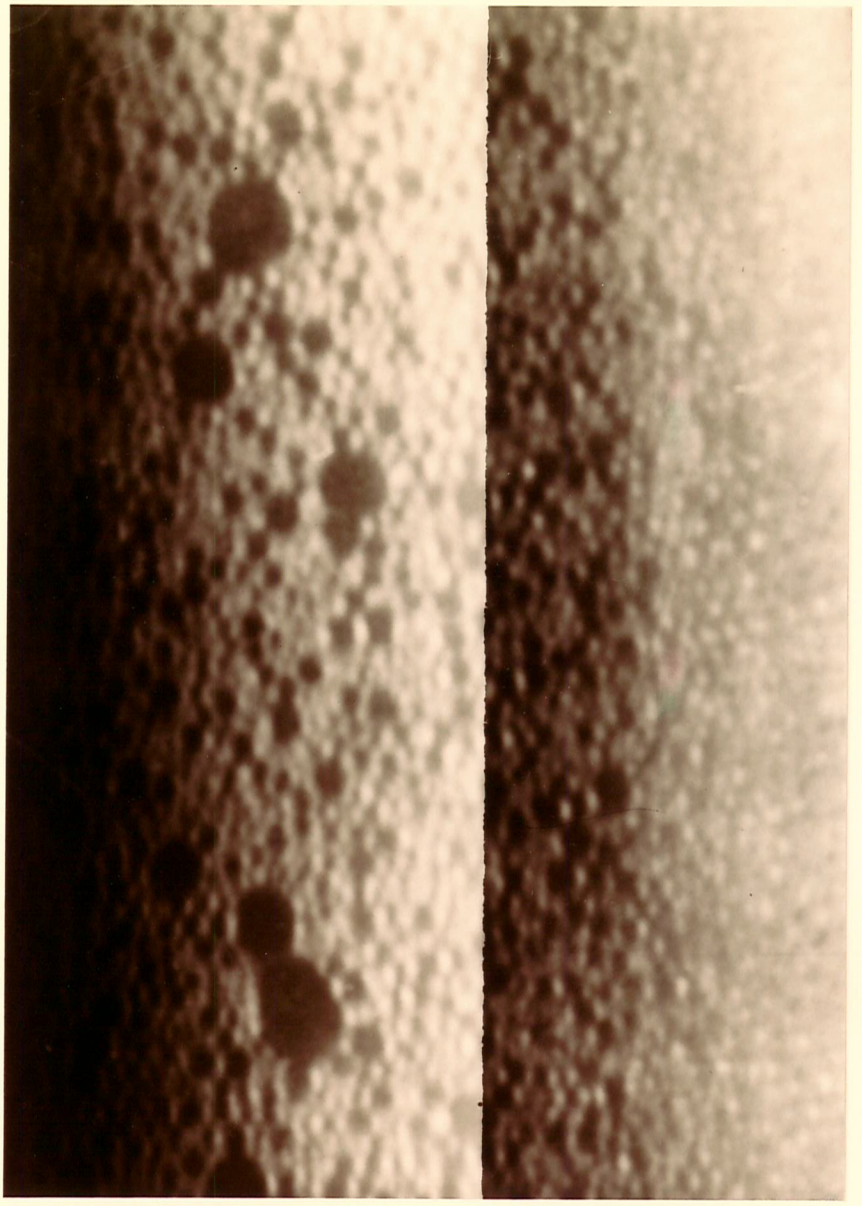

FIGURE 29. DIAGRAM OF PROPOSED FLOW REGIME FOR HIGH QUALITY FOAMS

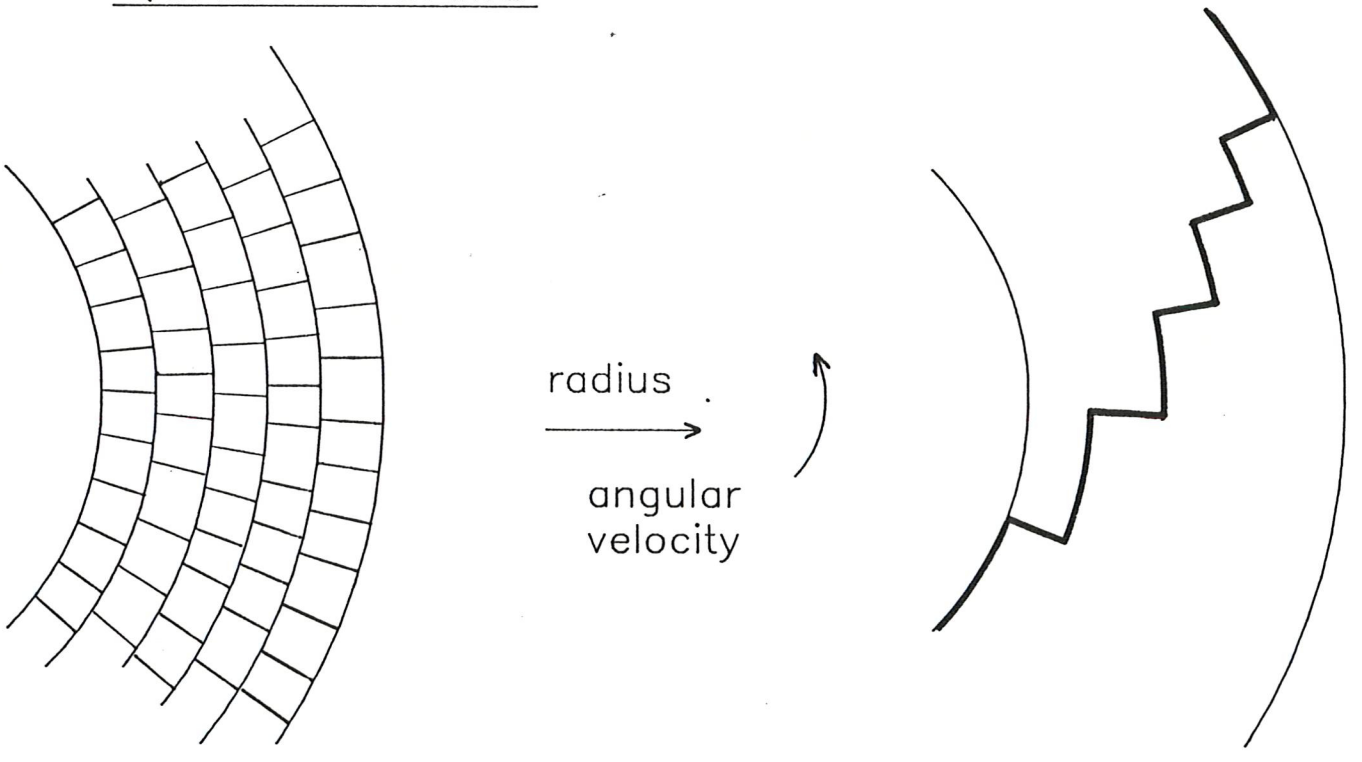

(a) Flowing structure of foam

(b) Velocity profile in the gap

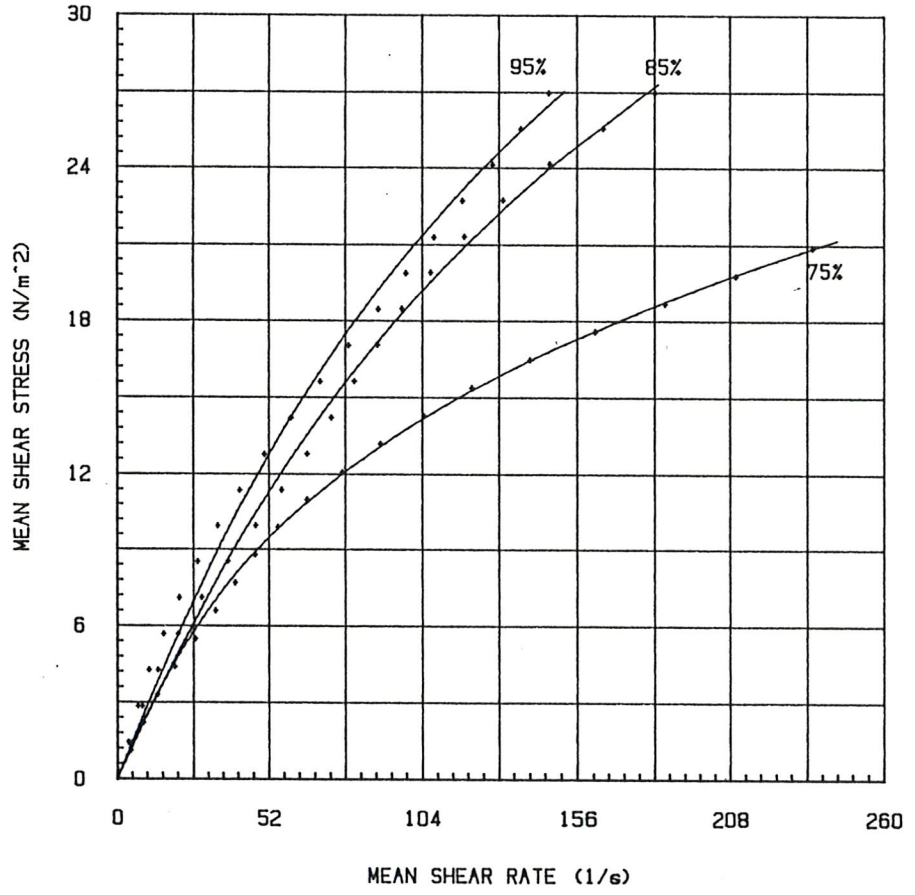

(a) Steiger-Ory description

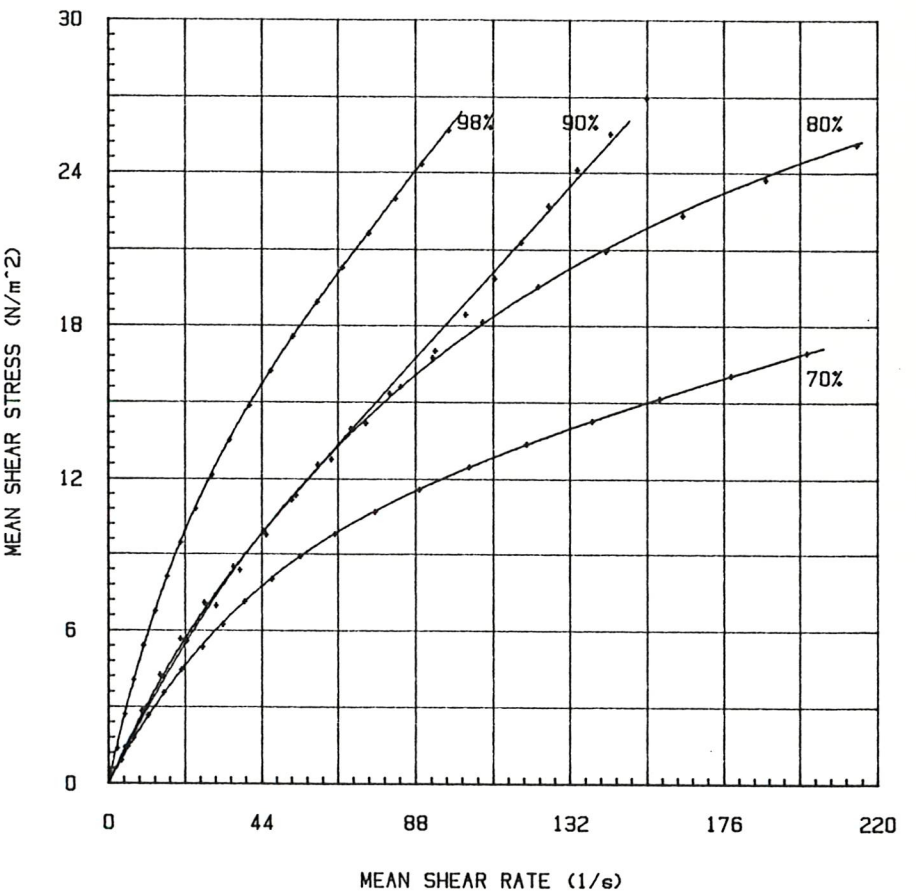

(b) 3-parameter description

FIGURE 30. EXAMPLES OF FITTING CURVES TO UNCORRECTED DATA FOR THE 20-21mm GAP

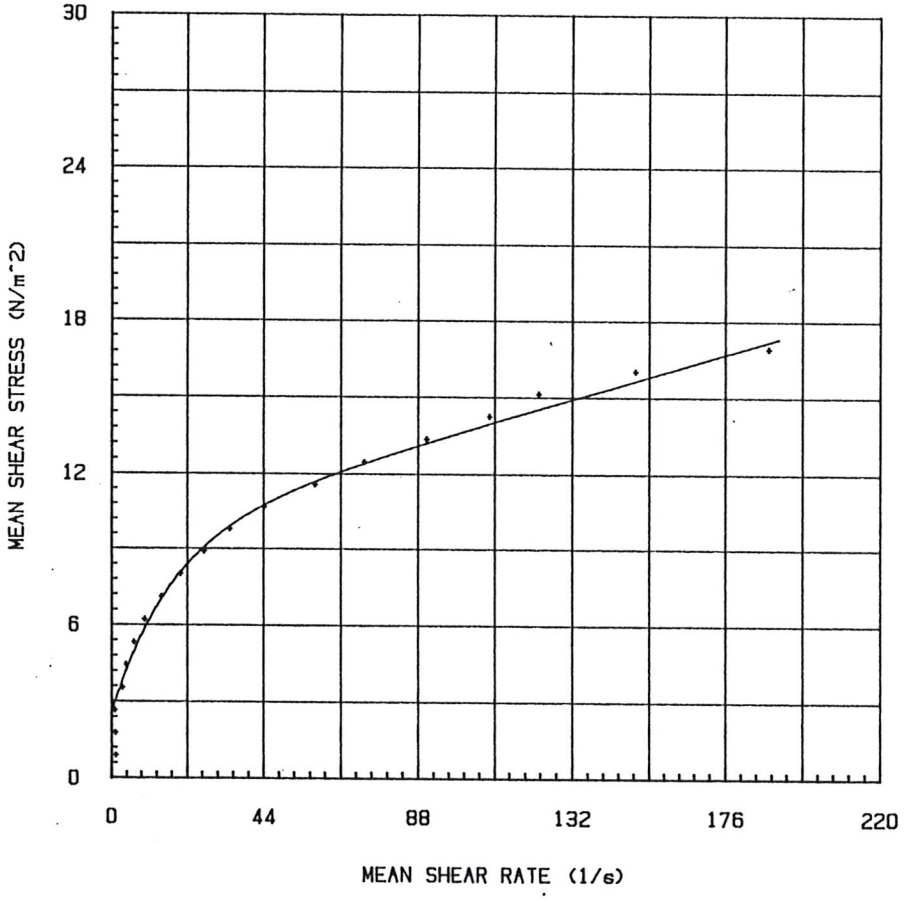

(a) 70% quality foam

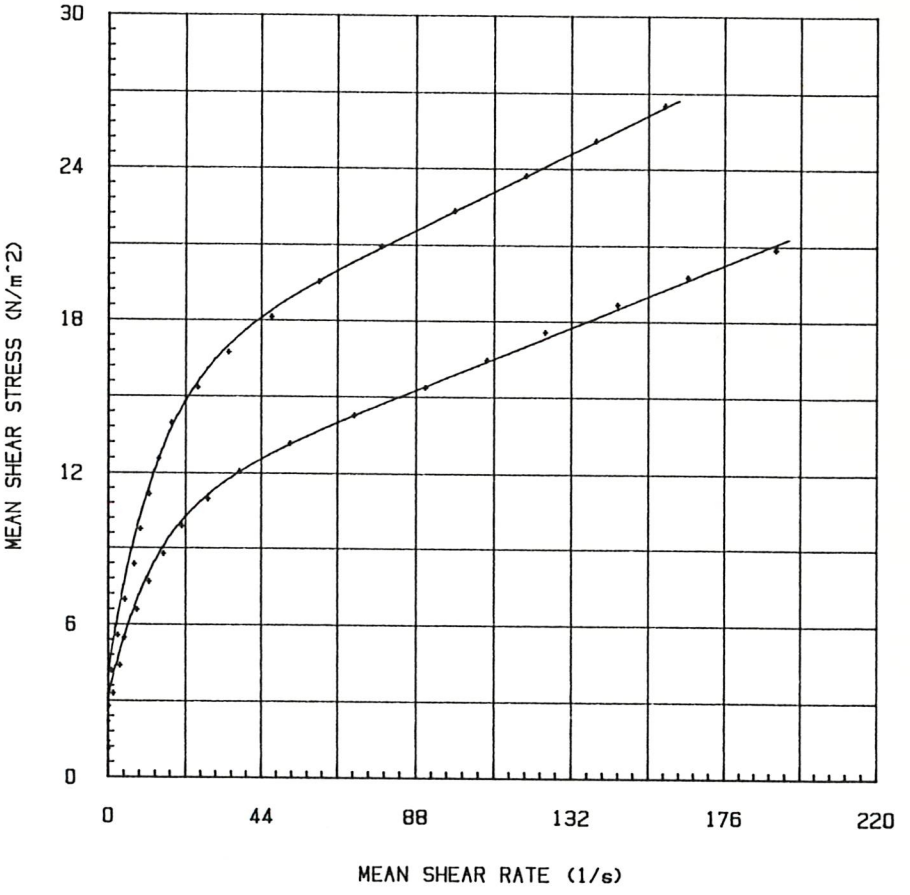

(b) 75% and 80% quality foam

FIGURE 31. EXAMPLES OF FITTING CURVES TO CORRECTED DATA FOR THE 20-21mm GAP

TABLE 1. BUBBLE SIZING DATA

FOAM QUALITY	NUMBER OF BUBBLES CROSSED BY EACH CHORD 1	2	3	4	5	6	7	8	9	10	n	$d=4z/\pi$ (μm)
70	24	27	26	26	24	–	–	–	–	–	25.4	125
75	25	21	20	22	22	23	22	22	23	23	22.3	143
80	17	16	18	16	15	17	16	16	18	17	16.6	192
85	16	14	16	14	15	15	15	15	14	17	15.1	210
90	14	15	15	14	14	15	13	15	12	13	14.0	227
95	9	9	10	10	11	11	9	10	11	11	10.1	314

CHORD LENGTH = 2.5mm (scaled)

TABLE 2. YIELD STRESS VALUES

(estimated from the corrected rheograms)

FOAM QUALITY (percent)	YIELD STRESS (N/m^2)
70	2.5
75	3.0
80	4.0
85	1.5
90	2.0
95	2.0
98	3.0

TABLE 3. CALCULATED MAXIMUM SLIP LAYER THICKNESSES

After Heller and Kuntamukkula (1)

FOAM QUALITY	BUBBLE RADIUS(μm)	BUBBLE WALL WIDTH(μm)	MAX.SLIP LAYER WIDTH(μm)
70	63	7.1	21.9
75	72	6.6	20.4
80	86	6.2	19.1
85	105	5.5	17.1
90	114	3.9	12.0
95	157	2.7	8.0
98	173 *	1.2	3.3

* Extrapolated value

TABLE 4. STEIGER–ORY CURVE FITTING PARAMETERS ($\dot{\gamma} = a\tau^3 + c\tau$)

(Uncorrected flow data)

FOAM	GAP	a	c
70%	A	0.0268	4.12
70%	B	0.0347	3.91
70%	C	0.0365	1.99
75%	A	0.0167	4.01
75%	B	0.0151	3.89
75%	C	0.0181	2.22
80%	A	0.0080	3.45
80%	B	0.0081	3.51
80%	C	0.0086	1.67
85%	A	0.0034	4.20
85%	B	0.0041	3.96
85%	C	0.0040	2.27
90%	A	0.0014	4.78
90%	B	0.0029	3.23
90%	C	0.00093	2.63
95%	A	0.0027	3.65
95%	B	0.0026	2.98
95%	C	0.00096	2.27
98%	A	0.0027	2.13
98%	B	0.0027	2.15
98%	C	0.0018	1.36

TABLE 5. CURVE FITTING PARAMETERS

EQU. $\tau=(\tau_b+\eta\dot{\gamma})(1-e^{-\xi\dot{\gamma}})$

(Uncorrected flow data)

FOAM/GAP	τ (N/m^2)	η (Pa.s)	ξ
70%/A	9.13	0.0395	0.0281
70%/B	8.52	0.037	0.0307
70% C	8.39	0.0423	0.0512
75%/A	12.52	0.0360	0.0201
75%/B	14.85	0.0281	0.0172
75%/C	9.75	0.0555	0.0479
80%/A	20.88	0.0274	0.0133
80%/B	17.71	0.0368	0.0163
80%/C	14.48	0.0597	0.0363
85%/A	5.35	0.126	0.0625
85%/B	11.5	0.0866	0.0246
85%/C	37.77	−0.0311	0.0111
90%/A	3.25	0.153	0.0880
90%/B	6.02	0.156	0.0657
90%/C	2.43	0.286	0.281
95%/A	8.60	0.144	0.0766
95%/B	6.02	0.169	0.0766
95%/C	3.30	0.304	0.267
98%/A	8.60	0.176	0.0717
98%/B	9.24	0.170	0.0593
98%/C	6.63	0.309	0.178

TABLE 6. CURVE FITTING PARAMETERS

EQU. $\tau = \tau_y + (\tau_b + \eta\dot{\gamma})(1 - e^{-\xi\dot{\gamma}})$

(Corrected flow data)

	FOAM QUALITY		
	70%	75%	80%
τ (N/m^2)	2.5	3.1	4.0
τ (N/m^2)	7.1	7.2	11.5
η (Pa.S)	0.0405	0.0565	0.069
ξ	0.060	0.085	0.080